Epstein-Barr virus promotes T cell dysregulation in a humanized mouse model of multiple sclerosis

Jessica R. Allanach[1], Naomi M. Fettig[1], Blair K. Hardman[1], Vina Fan[1], Ariel R. Rosen[1], Erin J. Goldberg[1], Zachary J. Morse[1], Iryna Shanina[1], Galina Vorobeychik[2,3], Lisa C. Osborne[1], Marc S. Horwitz[1*]

[1] Department of Microbiology and Immunology, The University of British Columbia, Vancouver BC, Canada

[2] Fraser Health Multiple Sclerosis Clinic, Burnaby BC, Canada

[3] Division of Neurology – Department of Medicine, University of British Columbia, Vancouver BC, Canada

[*] **Corresponding**:

Marc S. Horwitz

Life Sciences Centre, Office 3551

2350 Health Sciences Mall

University of British Columbia

Vancouver, B. C., Canada V6T 1Z3

604-822-6298

mhorwitz@mail.ubc.ca

Key terms: Humanized mice, peripheral blood mononuclear cell, Epstein-Barr virus infection, risk factor, multiple sclerosis, experimental autoimmune encephalomyelitis, immunomodulation, T cell proliferation, T cell regulation

Author contributions: JRA designed and performed experiments, analyzed data, and prepared the manuscript. NMF designed and performed ex vivo cellular assays. BKH designed and performed immunofluorescent imaging analysis. VF performed serum ELISAs. ARR performed myelin staining and quantification. NMF and EJG produced rhMOG protein. EJG and ZJM facilitated donor sample collection. IS coordinated phlebotomy, mouse breeding, and aided with in vivo procedures. JRA, NMF, BKH, VF, ARR, EJG, ZJM, and IS processed tissues for cellular analysis. GV recruited and assessed donors with RRMS and provided input for the study design. LCO oversaw immunofluorescent imaging and ex vivo cellular assays and provided input for the study design. JRA and MSH conceptualized the study, designed the methodology and interpreted results for discussion. MSH oversaw the study and manuscript preparation.

Itemized contributions:

Conceptualization – JRA, MSH

Investigation – JRA, NMF, BKH, VF, ARR, ZJM, EJG, IS, GV

Methodology – JRA, NMF, BKH, LCO, GV, MSH

Visualization – JRA, NMF, BKH

Writing - original draft – JRA

Writing - review and editing – JRA, NMF, BKH, LCO, MSH

Resources – LCO, GV, MSH

Supervision – LCO, GV, MSH

Funding acquisition – GV, MSH

Funding sources: The study was supported by grants and scholarships from the Multiple Sclerosis Society of Canada (MSSC, grant ID #3631), including the endMS personnel award program (JRA, NMF), the University of British Columbia (UBC), including the UBC 4YF award (BKH, ZJM), the Canadian Institutes of Health Research (CIHR, grant ID #168967, #178298), and the National Multiple Sclerosis Society (NMSS, grant ID #PP-1707-28236). The funders had no role in study design, data collection and interpretation, or the decision to submit the work for publication.

Declaration of interests: The authors declare no competing financial interests.

Acknowledgements: The authors thank the following individuals for their contributions to the study: Soren Gantt and Karen Simmons for providing the EBV *BALF5* qPCR protocol; John Priatel for providing the B95-8 EBV^{+} cell line; Jennifer Gommerman, Nancy Ruddle and Christopher Linington for providing the rhMOG-producing *E. coli* plasmid; Angela Lin, Guillermo Caballero, Natalie Strynadka, and Michael Murphy for assistance with rhMOG protein production; Tanya Kadach for organizing blood donations at the Fraser Health MS Clinic; the staff at the Modified Barrier Facility for animal husbandry; Yu Gu for ELISA protocol development; Brankica Culibrk and Philma Molina for phlebotomy; Justin Wong and Andrew Johnson for assistance with FACS; Virginie Jean-Baptiste and Isobel Mouat for assistance with animal monitoring. The authors acknowledge and are thankful for technical support from the Life Sciences Institute Cores (ubcFLOW) supported by the UBC GREx Biological Resilience Initiative. The authors express their gratitude to the blood donors for providing their time and samples to the study.

SUMMARY

In a novel humanized mouse model of multiple sclerosis (MS), donor history of Epstein-Barr virus (EBV) infection exacerbates disease severity by skewing the balance of effector and regulatory T cells in the brain and spinal cord. These results reveal an immunomodulatory mechanism by which latent EBV infection could predispose to the development of autoimmune disease.

ABSTRACT

Infection with the human-tropic Epstein-Barr virus (EBV) is a strong risk factor for multiple sclerosis (MS), though the underlying mechanisms remain unclear. To investigate the immunomodulatory effects of latent EBV infection, we induced experimental autoimmune encephalomyelitis (EAE) in immunocompromised mice humanized with peripheral blood mononuclear cells (PBMCs) from individuals with or without a history of EBV infection and/or a diagnosis of relapsing MS. HuPBMC EAE mice generated from EBV seronegative healthy donors were less susceptible to developing severe clinical disease than EBV seropositive healthy donor and RRMS cohorts. Donor EBV seropositivity and RRMS led to a significant incremental increase in the number of brain and spinal cord infiltrating effector T cells, in the absence of viral reactivation, due to enhanced proliferation of donor T cells and reduced regulatory T cell expansion. The data indicate that a history of EBV infection, further compounded by a diagnosis of RRMS, promotes T cell-mediated disease in a novel humanized mouse model of MS.

88 **INTRODUCTION**

89

90 Multiple sclerosis (MS) is an autoinflammatory disease of the central nervous system (CNS)
91 characterized by lesions of demyelinated nerve axons, infiltration of autoreactive T cells, and subsequent
92 neurodegeneration (Dendrou, Fugger and Friese, 2015). Clinical presentation among affected individuals
93 is heterogeneous, with variable symptoms and disease courses ranging from relapsing-remitting (RRMS)
94 to progressive forms with intermediate phenotypes (Klineova and Lublin, 2018). Symptoms also vary
95 widely but typically involve some combination of loss of coordination and sensation, muscle weakness,
96 vision impairment, fatigue, pain, cognitive impairment, and others (Compston and Coles, 2008). MS is
97 especially prevalent among women, for whom there is a heavy bias in incidence (Rommer *et al.*, 2020).
98 Although the exact etiology of MS is unclear, development of the disease is thought to be a consequence
99 of environmental triggers in genetically susceptible individuals (Olsson, Barcellos and Alfredsson, 2017).
100 The environmental factor most strongly and consistently linked to MS is infection with Epstein-
101 Barr virus (EBV) (Ascherio *et al.*, 2001; DeLorenze *et al.*, 2006; Thacker, Mirzaei and Ascherio, 2006;
102 Handel *et al.*, 2010; McKay *et al.*, 2016; Bjornevik *et al.*, 2022; Lanz *et al.*, 2022). EBV is a human
103 gammaherpesvirus transmitted through saliva that infects over 90% of all adults (Hjalgrim, Friborg and
104 Melbye, 2007). During acute infection the virus infects epithelial cells in the oropharynx and subsequently
105 disseminates and infects memory B cells, within which the virus establishes latency and persists for the
106 life of the host (Hjalgrim, Friborg and Melbye, 2007; Chaganti *et al.*, 2009). EBV reactivates intermittently
107 to transmit to new cells and hosts but is typically quiescent and, in healthy individuals, does not cause
108 disease. However, EBV is associated with a broad spectrum of malignancies and diseases (Hjalgrim,
109 Friborg and Melbye, 2007; Chen, 2011). The varied pathological consequences of EBV infection are
110 considered to be due to host-specific differences in immune responses to infection dictated by age, genetic

111 predispositions, and confounding environmental exposures (Hjalgrim, Friborg and Melbye, 2007; Balfour
112 *et al.*, 2013; Houldcroft and Kellam, 2015; Sallah *et al.*, 2020; Chen *et al.*, 2022). Acute infection is usually
113 asymptomatic when the virus is acquired at an early age, but delayed acquisition can cause infectious
114 mononucleosis (IM); a self-limiting clinical condition marked by a large expansion of $CD8^+$ T cells
115 specific to viral antigens (Dunmire, Hogquist and Balfour, 2015). The connection between EBV infection
116 and MS was first posited due to the prominent epidemiological overlap in cases of IM and MS (Warner
117 and Carp, 1981). Numerous studies have since provided evidence linking EBV infection with the
118 development of MS (Ascherio *et al.*, 2001; DeLorenze *et al.*, 2006; Thacker, Mirzaei and Ascherio, 2006;
119 McKay *et al.*, 2016; Bjornevik *et al.*, 2022; Lanz *et al.*, 2022).

120 Individuals who are EBV seronegative (EBV^-) have a relatively low risk for MS, whereas
121 asymptomatically infected individuals have a moderate risk, and those who have previously developed
122 IM have a significantly higher risk for MS than those who acquired the virus asymptomatically (Thacker,
123 Mirzaei and Ascherio, 2006; Handel *et al.*, 2010). Additionally, nearly all adult and pediatric MS patients
124 are EBV seropositive (EBV^+) (Alotaibi *et al.*, 2004; Banwell *et al.*, 2007; Levin *et al.*, 2010), and MS
125 patients show higher EBV-specific antibody titers than age-matched controls in the years preceding
126 disease onset (DeLorenze *et al.*, 2006). MS patients also show increased frequencies of EBV-specific T
127 cells in the blood compared to unaffected individuals with a similar viral load, some of which are cross
128 reactive to myelin epitopes (Lünemann *et al.*, 2006, 2008; Lanz *et al.*, 2022). Recently, a longitudinal
129 case-matched study demonstrated a 32-fold increased risk for MS and significant upregulation of a
130 biomarker of axonal degeneration in individuals with MS, specifically following EBV seroconversion in
131 young adulthood (Bjornevik *et al.*, 2022). The efficacy of B cell depletion therapies in MS patients further
132 suggests a role for EBV infection in disease, as anti-CD20 antibodies may target the viral reservoir
133 (Jagessar *et al.*, 2013). Moreover, EBV infection is associated with the development of other autoimmune

134 diseases, including rheumatoid arthritis and systemic lupus erythematosus (Balandraud and Roudier,
135 2018; Jog and James, 2021), which suggests a common mechanism by which EBV predisposes for
136 autoimmunity. Latent gammaherpesvirus infection is known to modulate immune responses relevant to
137 autoimmunity, including downregulation of B cell apoptosis, suppression of regulatory T cell (Treg)
138 function and production of an interferon-I response (Gasper-Smith, Marriott and Bost, 2006; Quan *et al.*,
139 2010; Pratt, Zhang and Sugden, 2012). Despite mounting epidemiological and clinical evidence
140 suggesting EBV infection is a causative factor in MS, experimental investigation of mechanism has been
141 limited due to the high prevalence of EBV in the general population, the preponderance of asymptomatic
142 EBV infection years prior to MS onset, and, since EBV exclusively infects humans, a lack of suitable
143 animal models.

144 Due to the narrow tropism of latent EBV for human B cells, and resulting inability to infect rodent
145 immune cells, the animal models that have helped shaped our understanding of MS pathogenesis are not
146 amenable to EBV infection directly. To address this species limitation, our group previously developed a
147 mouse model wherein wild-type C57Bl/6 mice are latently infected with the rodent homolog of EBV,
148 gammaherpesvirus 68 (γ-HV68), and induced with experimental autoimmune encephalomyelitis (EAE),
149 a widely used autoimmune model of MS, to mimic the viral acquisition observed in humans years prior
150 to disease onset (DeLorenze *et al.*, 2006; Miller, Karpus and Davidson, 2007; Olivadoti *et al.*, 2007;
151 Casiraghi *et al.*, 2012, 2015; Bjornevik *et al.*, 2022). Mice latently infected with γ-HV68 prior to EAE
152 induction experience a severe pathology more alike MS than uninfected EAE mice (Casiraghi *et al.*, 2012,
153 2015). The enhanced MS-like disease is characterized by greater clinical scores with earlier symptom
154 onset, as well demyelinated lesion formation in the brain, and CNS infiltration of activated
155 macrophages/microglia, cytotoxic $CD8^+$ T cells, and Th1-skewed $CD4^+$ T cells (Casiraghi *et al.*, 2012).
156 Treg frequencies are also significantly decreased in the CNS and spleens of infected EAE mice (Casiraghi

157 *et al.*, 2012). Moreover, these effects were exclusive to latent γ-HV68 infection, as acute γ-HV68 infection
158 and chronic infection with other viruses, including murine cytomegalovirus and lymphocytic
159 choriomeningitis virus, were not able to enhance EAE (Casiraghi *et al.*, 2012). The immunopathological
160 features of the γ-HV68/EAE model are hallmark characteristics of MS that are either far less pronounced
161 or absent in classical EAE models (Simmons *et al.*, 2013; Wagner *et al.*, 2020), which strongly indicates
162 EBV might contribute to similar aspects of the pathogenesis of MS in humans. Although this modeling
163 approach has been educational, a more complete understanding of how EBV modifies MS susceptibility
164 could be gained from improved models of host-viral interactions.

165 Here, we sought to study the role of EBV latency in MS using humanized mice that contain
166 reconstituted human immune systems naturally exposed to EBV. EBV infection of humanized mice has
167 recapitulated various aspects of the viral immune response and pathogenesis of EBV-associated diseases
168 observed in humans, including lytic and latent infections (Melkus *et al.*, 2006; Yajima *et al.*, 2008; Lin *et*
169 *al.*, 2015), lymphoproliferation and tumor formation (Islas-Ohlmayer *et al.*, 2004; Lim *et al.*, 2007; Heuts
170 *et al.*, 2014), among others (Kuwana *et al.*, 2011; Sato *et al.*, 2011; Münz, 2015). Studies of EBV infection
171 in humanized mice, however, have not reported CNS-localized inflammation leading to motor deficits, as
172 seen in classical EAE models of MS. To capture the effects of long-term latent EBV infection on immune
173 function and neuroinflammation, we induced EAE in immunodeficient mice reconstituted with peripheral
174 blood mononuclear cells (PBMCs) isolated from healthy EBV^+ or EBV^- adults. Since the vast majority of
175 people living with MS are EBV^+ (Levin *et al.*, 2010; Abrahamyan *et al.*, 2020), we also tested donor
176 PBMCs from this group for neuroinflammatory potential in EAE. Supporting a role for EBV-mediated
177 immunomodulation in MS susceptibility, we found that donor EBV serostatus clearly defined the time of
178 EAE symptom onset and severity of disease. Further, this novel mouse model revealed that PBMCs from
179 EBV seropositive donors led to diminished regulatory T cell expansion and enhanced effector T cell

180 infiltration of the CNS, providing new mechanistic understanding of how latent EBV infection promotes

181 CNS autoimmunity.

182 **RESULTS**

183

184 **EBV seropositive and RRMS donor derived PBMCs exacerbate clinical disease severity in**

185 **HuPBMC EAE mice**

186 To evaluate the impact of EBV infection on clinical outcomes of disease in a humanized MS
187 model, we engrafted NOD/SCID-IL2Rγ $^{-/-}$ (NSG) mice with PBMCs (HuPBMC mice) from three donor
188 groups based on EBV seropositivity and RRMS diagnosis (Figure 1A). For this study, we enrolled
189 treatment naïve female donors aged 19–39, due to the increased prevalence of RRMS among young
190 women (Rommer *et al.*, 2020). Consistent with previous reports (DeLorenze *et al.*, 2006; Mouhieddine *et*
191 *al.*, 2015; Bjornevik *et al.*, 2022), the donors diagnosed with RRMS were all EBV seropositive (EBV^{+})
192 and exhibited significantly elevated EBV-specific serum IgG titres to both the acute phase viral capsid
193 antigen (VCA, Figure 1B) and the latent phase Epstein-Barr nuclear antigen 1 (EBNA-1, Figure 1C)
194 compared to previously infected, otherwise healthy EBV^{+} donors. Uninfected EBV seronegative (EBV^{-})
195 healthy donors (HDs) were identified and grouped based on the absence of serum IgM and IgG specific
196 to both antigens. EBV viral load analysis of donor PBMCs confirmed that none of the donors had
197 detectable levels of cell-associated EBV that might be indicative of a highly active infection or an EBV-
198 associated disorder such as malignancy or infectious mononucleosis (Kimura *et al.*, 1999) (Figure 1D).
199 We also assessed donor group differences in other serological factors associated with MS (McKay *et al.*,
200 2016; Olsson, Barcellos and Alfredsson, 2017). Our donors showed 33–50% seropositivity for
201 cytomegalovirus (CMV) within each donor group, which reflects the general population (Staras *et al.*,
202 2006; Lachmann *et al.*, 2018) (Table 1). Although there was no significant difference in anti-CMV IgG
203 titres between EBV^{+} HD and the other two groups, RRMS EBV^{+} donors had elevated anti-CMV IgG
204 compared to EBV^{-} HD (Figure S1A). We also verified that the donors did not have any existing overt

205 seroreactivity to the inducing antigen, recombinant human myelin oligodendrocyte glycoprotein (rhMOG,
206 Figure S1B), and the donor groups had statistically similar serum 25-OH vitamin D levels (Figure S1C).
207 Human leukocyte antigen (HLA) typing revealed that two of four RRMS donors expressed the MS risk
208 allele DRB1*15:01 (Wang *et al.*, 2020), whereas none of the healthy donors expressed this allele (Figure
209 S1D). Individual donor characteristics, including clinical MS parameters and viral serostatus, are reported
210 in Table 1.

211 Flow cytometric analysis of transplanted PBMCs confirmed that recipient NSG mice were
212 engrafted with a similar composition of immune cells from each donor (Figure S2). HuPBMC mice were
213 then induced with EAE using a mixture of rhMOG$_{1-120}$ and MOG$_{35-55}$ after a three-week reconstitution
214 period (Figure 1A). HuPBMC mice were found to be susceptible to EAE and exhibited symptoms typical
215 of other murine EAE models, including weight loss, piloerection, motor imbalance, and an ascending
216 paralysis with resolution within approximately a week from onset (data not shown and Figure S3, S7).
217 The development of paralysis, reaching EAE scores of up to 4 on a standard 5-point scale (Miller, Karpus
218 and Davidson, 2007), was similar to the asynchronous, relapsing EAE phenotype of the Non-Obese
219 Diabetic (NOD) background strain for the NSG (Figure S3, S7) (Baker *et al.*, 2019). HuPBMC EAE mice
220 demonstrated an exacerbation of clinical disease by multiple measures when engrafted with PBMCs from
221 donors who were EBV$^+$ and had been diagnosed with RRMS (Figure 1E – G). The overall disease course
222 of EAE was significantly worsened in EBV$^+$ HD mice compared to EBV$^-$ HD mice, which was in turn
223 significantly more severe in the EBV$^+$ RRMS recipient cohorts compared to both HD groups (Figure 1E).
224 The incidence of EAE symptoms was significantly greater in EBV$^+$ RRMS recipient mice compared to
225 the HD groups, and moderately increased with EBV infection between HD groups (Figure 1F). HuPBMC
226 EAE mice derived from EBV$^-$ HD donors also exhibited a significantly delayed time to symptom onset
227 compared to the EBV$^+$ recipient groups, which was not significantly different between the EBV$^+$ recipient

228 groups, regardless of an RRMS diagnosis (Figure 1G). The clinical outcomes of EAE indicate that donor
229 EBV infection and RRMS diagnosis both increase disease susceptibility and severity in recipient
230 HuPBMC EAE mice.
231
232 **Human T cells infiltrate and localize to areas of inflammatory demyelination in the CNS of**
233 **HuPBMC EAE mice**
234 In classical EAE models, clinical disease scores are assessed based on the severity of ascending
235 paralysis, which is a consequence of inflammatory damage to the spinal cord (Simmons *et al.*, 2013). To
236 investigate the underlying cause of the clinical symptom differences associated with donor EBV and
237 RRMS status, we first evaluated the degree of demyelination of the spinal cord among the three recipient
238 HuPBMC EAE groups. EAE induction of immunocompetent NOD mice and RRMS/HD EBV^+ HuPBMC
239 mice led to a significant loss of total myelin content relative to unaffected NSG control mice (Figure 2A).
240 Both EBV^+ groups had significantly less myelin in the spinal cord compared to NSG controls, whereas
241 EAE induction of EBV^- HD recipient HuPBMC mice did not significantly reduce myelination, suggesting
242 greater protection from EAE consistent with diminished clinical disease severity in this group. As
243 demyelination in EAE is predominantly T cell driven (Furtado *et al.*, 2008; Hohlfeld and Steinman, 2017),
244 we confirmed that engrafted human T cells could infiltrate the CNS following induction. Notably, we
245 detected an accumulation of human $CD8^+$ T cells in the white matter of both the spinal cord (Figure 2B)
246 and the cerebellum (Figure 2C) of HuPBMC EAE mice engrafted with RRMS donor PBMCs,
247 demonstrating that engrafted human T cells can localize to CNS regions typically demyelinated in
248 classical EAE models. Moreover, we observed an inflammatory lesion within the cerebellum marked by
249 microgliosis, as indicated by concentrated Iba-1 staining, that co-localized with human $CD8^+$ T cell
250 infiltration (Figure 2D). Demyelination of the spinal cord and brain lesion infiltrates composed of

251 macrophages and $CD8^+$ T cells are consistent with the CNS immunopathology seen in both EAE models
252 and MS, respectively (Salou *et al.*, 2015; Wagner *et al.*, 2020).
253
254 **CNS immunopathology in HuPBMC EAE is mediated by human Th1 and cytotoxic T cells and**
255 **murine macrophages**
256 Murine EAE models can present with a range of distinct disease symptomologies, CNS
257 pathologies and constituent autoimmune processes based on the induction method and rodent strain used.
258 As this HuPBMC EAE model is novel, we first characterized the immunopathological features of EAE
259 mice using NSG mice engrafted with HD EBV^+ PBMCs, in order to establish a baseline from which to
260 compare EBV^- and RRMS PBMCs recipient cohorts. Consistent with our findings by histology, we
261 measured substantial spinal cord infiltration of both human $CD4^+$ ($hCD4^+$, 3802 ± 3525 cells/ spinal cord)
262 and $CD8^+$ ($hCD8^+$, 1225 ± 1262 cells/ spinal cord) T cells by flow cytometry in HuPBMC EAE mice
263 (Figure 3A). A large proportion of $hCD4^+$ T cells in the CNS produced IFNγ (~45%). Although there were
264 relatively few IL-$17A^+$ cells, the majority of these cells co-expressed IFNγ, indicating that this model is
265 predominantly Th1-driven (Figure 3A, B). Among CNS-infiltrating $hCD8^+$ T cells, ~80% expressed IFNγ
266 and/or Granzyme B (GzmB) (Figure 3A, B), suggesting they are capable of cytotoxic activity. Though the
267 level of T cell reconstitution and infiltration was variable among tissues derived from the same recipient
268 cohort, the pattern of cytokine expression was similar in the periphery and in the CNS (Figure 3B). Human
269 T cell infiltration was detected in the CNS of all EAE-induced HuPBMC mice regardless of the
270 development of clinically visible EAE symptoms (Figure S4). However, the spinal cords of mice that
271 developed clinical symptoms contained significantly greater numbers of $hCD45^+$ cells, including total
272 $hCD3^+$ and activated $hCD8^+$ T cells, than mice that remained subclinical (Figure S4). Moreover, there was
273 a significantly higher ratio of $hCD8^+$ T cells relative to $hCD4^+$ T cells within the CNS of mice with EAE

274 symptoms (Figure 3C), suggesting a critical role for cytotoxic hCD8^{+} T cells in mediating demyelination
275 and tissue damage.

276 Myelin phagocytosis by infiltrating and resident macrophages/microglia is a key mediator of
277 demyelination in EAE models (Yamasaki *et al.*, 2014; Dong and Yong, 2019). In humanized mouse
278 models, both endogenous murine and engrafted human myeloid cells reconstitute and can co-exist within
279 the CNS (Gorantla, Gendelman and Poluektova, 2012; Zhang *et al.*, 2021). We assessed the abundance of
280 murine (mCD45^{hi}CD11b^{hi}F4/80^{+}) and human (hCD45^{+}CD14^{+}CD68^{+}) macrophages in the CNS and
281 periphery to determine the potential relative contribution of each subset to the immunopathology of
282 HuPBMC EAE. Unlike hematopoietic stem cell engraftment-based humanized mouse models, PBMC
283 humanization of NSG mice generally favors the engraftment of T cells over innate immune subsets
284 (Morillon *et al.*, 2020). Accordingly, we observed numerous mCD45^{hi} macrophages in the brains, spinal
285 cords, and spleens of HuPBMC EAE mice but very few hCD45^{+} macrophages (Figure 3D). The overall
286 scarcity of hCD45^{+}CD14^{+}CD68^{+} cells in the CNS suggests that infiltrating murine macrophages and
287 resident microglia likely perform the bulk of axonal demyelination following EAE induction. We
288 confirmed that murine myeloid cells phagocytosed myelin in the HuPBMC EAE model based on the
289 detection of intracellular myelin basic protein (MBP) in mCD45^{hi} macrophages in the CNS after induction
290 (Figure 3E). In the spinal cord, the total number of infiltrating hCD8^{+} T cells correlated strongly and
291 specifically with the number of infiltrating MBP^{+} murine macrophages in the same tissue (Figure 3F),
292 similar to MS brain lesions wherein infiltrating cytotoxic T cells and macrophages are positively
293 correlated with the extent of axonal damage (Bitsch *et al.*, 2000). An association with myelin phagocytosis
294 was not observed for hCD4^{+} T cells or human macrophages (Figure S5). Furthermore, we observed a
295 significant increase in the total numbers of murine macrophages and myelin-phagocytosing microglia
296 (mCD45^{lo}CD11b^{hi}F4/80^{+}MBP^{+}) in the spinal cords of HuPBMC mice that developed clinical EAE

297 symptoms compared to mice that remained subclinical (Figure 3G, H), supporting the notion that murine
298 myeloid cells demyelinate the CNS sufficiently to produce clinical symptoms in this model.

299 Collectively, the data indicate that infiltrating hCD4$^+$ T cells direct a Th1 polarized response in the
300 CNS of HuPBMC EAE mice that leads to hCD8$^+$ T cell-mediated myelin damage and subsequent
301 phagocytosis by murine macrophages and microglia. The capability of hCD8$^+$ T cells to exert myelin-
302 directed cytotoxicity, however, was unclear in an interspecies model of immune-mediated demyelination.
303 Based on previous work, which has demonstrated productive human T cell receptor (TCR) interactions
304 with mouse major histocompatibility complex (MHC) in humanized NSG mice (Halkias *et al.*, 2015), we
305 assessed whether hCD8$^+$ T cells could effectively interact with myelin antigen presented on mouse MHC
306 I-expressing cells ex vivo (Figure 3I). Co-culture of sort-purified splenic mCD45$^+$ and hCD8$^+$ cells from
307 HuPBMC mice in the presence of rhMOG resulted in a significant expansion of mCD11c$^+$ cells, including
308 those expressing CD40, and a simultaneous decrease in CD8 median fluorescence intensity on human
309 CD3$^+$CD8$^+$ T cells (Figure 3J), indicative of increased antigen recognition (Kroger and Alexander-Miller,
310 2007). There was also a significant increase in the proportion of hCD8$^+$ T cells expressing the antigen
311 activation marker CD137, as well as IFNγ (Figure 3J), which affirms the functional capacity of hCD8$^+$ T
312 cells to recognize and respond to antigen in humanized mouse tissues. These data highlight the interspecies
313 nature of the immunopathology of the HuPBMC EAE model and supports its use as a model of MS.

314

315 **Donor EBV seropositivity and RRMS diagnosis promote effector T cell accumulation in the CNS**
316 **of HuPBMC EAE mice**

317 Since the HuPBMC EAE recipient groups showed an EBV and RRMS associated increase in
318 disease severity and demyelination, we sought to assess human immune cell infiltration of the CNS and
319 reconstitution in the periphery to identify contributing immune subsets. In the brain, spinal cord, and

320 spleen, HuPBMC EAE recipient cohorts followed a stepwise, increasing trend in total human $CD45^+$
321 immune cell counts with donor EBV seropositivity and RRMS diagnosis (Figure 4A). In all HuPBMC
322 EAE mice, relatively few human B cells infiltrated the CNS relative to T cells: approximately 25–100
323 $hCD19^+$ B cells versus 10^3–10^5 $hCD3^+$ T cells per spinal cord (Figure 4B, C). Total B cell infiltration of
324 the CNS and peripheral reconstitution also did not differ between the three recipient groups (Figure 4B).

325 EBV intermittently reactivates from latently infected memory B cells to transmit to new cells
326 (Hadinoto *et al.*, 2008), which has been suggested to potentially contribute to relapses in MS (Bar-Or *et*
327 *al.*, 2020). Though engrafted B cells reconstituted the spleen (approximately 10^3 – 10^5 $hCD19^+$ B cells),
328 EBV viral genomes were undetectable in the spleens of most mice at EAE endpoint, regardless of recipient
329 group (Figure 4D), indicating peripheral viral reactivation from engrafted B cells is unlikely to have
330 influenced disease outcomes. We further assessed whether an active EBV infection may play a role in
331 promoting disease by measuring antibody production by EBV-specific B cells. Given that engrafted
332 lymphocytes do not form organized germinal centers in NSG mouse lymphoid tissues, and are
333 subsequently unable to promote class-switching and hypermutation of human B cells (Jangalwe *et al.*,
334 2016; Lang *et al.*, 2017), any EBV-specific IgG produced in these mice would indicate a reactivation of
335 engrafted memory B cells rather than a novel response to infection post-engraftment. We confirmed the
336 production of rhMOG-specific human IgM and the absence of rhMOG-specific human IgG in the serum
337 of HuPBMC EAE mice (Figure S6A), indicating the engraftment of otherwise functionally responsive
338 human B cells. In three separate EBV^+ recipient cohorts, no human IgG to the EBV antigen VCA could
339 be detected in serum after EAE induction (Figure S6B), despite a strong response in corresponding donor
340 serum (Figure 1B), suggesting that, under these conditions, an active infection likely does not play a role
341 in the enhancement of clinical disease.

342 Though direct B cell involvement in causing disease differences seemed improbable, total hCD3$^+$
343 T cell counts comprised the majority of infiltrating human CD45$^+$ cells in the CNS, following the same
344 increasing trend of higher counts with donor EBV and RRMS status (Figure 4C). Among infiltrating T
345 cells, hCD4$^+$ T cells demonstrated a consistent increase in total counts in all three tissues with donor EBV
346 seropositivity and RRMS (Figure 4E), while hCD8$^+$ T cell counts were increased only in the brain of
347 RRMS recipient mice compared to HD mice (Figure 4F). Increased hCD8$^+$ T cell counts in the RRMS
348 recipient brains corresponded to greater numbers of infiltrating murine immune cell in these samples
349 (Figure S6C), whereas microglia and human macrophage counts did not differ between recipient groups
350 in any tissue (Figure S6D, E). Splenic reconstitution of hCD8$^+$ T cells was also similar between groups
351 (Figure 4F).

352 Among hCD4$^+$ T cells, the proportions of cells expressing cytokines indicative of subset skewing
353 (Th1 and Th17) did not follow any consistent trends with PBMC donor EBV or RRMS status (Figure 5A,
354 S7A – C), indicating polarization toward a particular inflammatory Th subset was not the main driver of
355 clinical group differences. However, the increased number of total hCD4$^+$ T cells in EBV$^+$ HD and RRMS
356 recipient group tissues than EBV$^-$ HD tissues (see Figure 4E) led to an overall greater abundance of
357 effector Th1 cells in the CNS and spleen (Figure 5B), despite similar levels of IFNγ expression (Figure
358 5A, S7A). The relatively fewer total numbers of Th17 (Figure 5C) and IFNγ$^+$IL-17A$^+$ Th cells (Figure
359 5D) showed some moderate, but not striking group specific trends that would otherwise suggest they
360 underpinned the observed clinical disease differences. Despite similar numbers of total infiltrating hCD8$^+$
361 T cells in the CNS between recipient cohorts (see Figure 4F), donor EBV seropositivity led to significantly
362 enhanced T cell cytotoxicity (Figure 5E), as measured by a significant shift from less IFNγ expression
363 (Figure 5F) to more GzmB expression (Figure 5G, H) among hCD8$^+$ T cells in the brain and spinal cord.
364 Interestingly, this trend was not further enhanced by donor RRMS diagnosis. Although total effector

365 hCD8$^+$ T cell counts were similar between recipient group tissues (Figure S7D – F), the skewing toward
366 increased cytotoxic capacity within the infiltrating hCD8$^+$ T cell population is consistent with the elevated
367 level of demyelination in the CNS of EBV$^+$ recipient mice (see Figure 2A). Overall, both a donor history
368 of EBV infection and a diagnosis of RRMS led to incremental increases in the accumulation of pathogenic
369 effector hCD4$^+$ and hCD8$^+$ T cells in the CNS of HuPBMC mice induced with EAE.
370

371 **Donor EBV seropositivity and RRMS diagnosis limit regulatory T cell expansion in HuPBMC**
372 **EAE mice**

373 Alongside greater Th1 and cytotoxic T effector cell infiltration of the CNS, we observed a
374 reduction in the proportion of hCD4$^+$ T cells expressing the regulatory transcription factor FOXP3 in EBV$^+$
375 recipient group tissues compared to the EBV$^-$ HD group (Figure 6). Initially, FOXP3 expression in hCD4$^+$
376 T cells from freshly isolated PBMCs is comparable between donor groups (Figure 6A) but is incrementally
377 reduced in EBV$^+$ HD and RRMS hCD4$^+$ T cells in the blood of NSG mice following engraftment of the
378 PBMCs (Figure 6B). Following EAE induction, this trend of lower proportions of FOXP3$^+$ T cells is
379 likewise observed in the CNS and spleen of EBV$^+$ HD and RRMS recipient mice (Figure 6C – E), even
380 though total regulatory T cell (Treg) counts are similar between groups (Figure S6F). The sum
381 consequence of this incremental increase in pathogenic T cell infiltration of the CNS and simultaneous
382 suppression of Treg expansion was a significantly greater ratio of effector hCD4$^+$ and hCD8$^+$ T cells to
383 regulatory hCD4$^+$ T cells in the CNS and periphery of EBV$^+$ HD and RRMS recipient mice compared to
384 EBV$^-$ HD mice (Figure 6F, G & S6G, H). As sample collection was timed to maintain similar overall
385 cumulative EAE scores between groups at endpoint, differences in CNS infiltration could not be correlated
386 with greater clinical disease burden for RRMS and EBV$^+$ recipient groups (Figure S8A – D). Though
387 weight loss followed the EBV and RRMS status trend with clinical disease severity (Figure S8E), the

388 incidence of clinical symptoms of graft-versus-host disease (GvHD) was comparably low between the
389 groups (Figure S8F, G), suggesting excessive, nonspecific inflammation due to varying degrees of human
390 PBMC recognition of murine MHC within the recipient tissues was not the main determinant of the
391 observed Th1 expansion and Treg suppression. The data collectively suggest that a history of both EBV
392 infection and an RRMS diagnosis among donors leads to a compounded reduction in the expansion of
393 Tregs and a concomitant increase in effector Th1 and cytotoxic T cell abundance, and, subsequently, to
394 systemic dysregulation of T cell-mediated inflammation resulting in excessive CNS damage and worsened
395 clinical outcomes.
396
397 **EBV infection and RRMS both enhance donor T cell proliferation following TCR stimulation**
398 Based on the findings above, PBMCs from EBV^- HD are seemingly less reactive to myelin antigen
399 challenge in the HuPBMC EAE model than EBV^+ HD and RRMS PBMCs. The observation that FOXP3
400 expression among $hCD4^+$ T cells is reduced even prior to EAE induction suggests the effector T cells may
401 become more activated during reconstitution due to a lack of regulation, which then transfers to the CNS
402 after MOG immunization. Within the donor PBMCs (prior to engraftment into NSG mice), $hCD4^+$ and
403 $CD8^+$ T cells did not differ in their group baseline expression of the activation markers HLA-DR, CD38,
404 CD137, or CD154 (Figure S9), nor of subset-specific transcription factors (Figure S10). Likewise,
405 baseline cytokine expression did not follow any EBV or RRMS associated trends that would explain the
406 observations in the HuPBMC EAE mice (Figure S10). To evaluate the possibility that T cells from an
407 EBV-exposed host are intensely activated following TCR engagement generally, we stimulated donor
408 PBMCs by anti-hCD3/CD28 stimulation in vitro (Figure 7). Interestingly, direct stimulation of the TCR
409 without a specific antigen resulted in a trend of enhanced $hCD4^+$ T cell proliferation with donor EBV and
410 RRMS status, as measured by a CFSE-based proliferation index and Ki-67 expression (Figure 7A – C).

411 hCD4$^+$ T cells from EBV$^+$ HD PBMCs, and even more so EBV$^+$ RRMS PBMCs, were able to attain a
412 higher average number of cellular divisions during the incubation period compared to EBV$^-$ donor PBMCs
413 (Figure 7B). Consistent with the HuPBMC EAE model data, these T cells were not differentially polarized
414 after stimulation based on inflammatory cytokine expression (Figure 7D, E). Moreover, the same effects
415 were observed with hCD8$^+$ T cells, as measured by an incremental increase in proliferation with donor
416 EBV seropositivity and RRMS diagnosis following anti-CD3/CD28 treatment (Figure 7F – H). Stimulated
417 hCD8$^+$ T cell cytokine expression also did not follow group specific trends (Figure 7I, J). Therefore, in
418 addition to an EBV and RRMS associated deficiency in the expansion of regulatory T cells in the
419 HuPBMC EAE model, both hCD4$^+$ and hCD8$^+$ T cells from EBV experienced hosts are also more
420 proliferative following general TCR stimulation, without alteration to the polarization profiles of these
421 cells.

422 **DISCUSSION**

423

424 The findings of this study highlight the utility of PBMC-humanized EAE mice in modelling
425 clinical and immunopathological aspects of MS and its association with a history of EBV infection.
426 Immunocompromised NSG mice engrafted with human donor PBMCs were susceptible to the
427 development of EAE symptoms and demyelination, much like classical murine EAE models immunized
428 with myelin antigens. As confirmed by histological analysis, engrafted human $CD8^+$ T cells were able to
429 migrate to and infiltrate the mouse CNS and localize to areas of microgliosis and myelin damage.
430 Moreover, the CNS of symptomatic mice was enriched for $hCD8^+$ relative to $hCD4^+$ T cells, which is
431 commonly observed in post-mortem analysis of MS lesions (Babbe *et al.*, 2000; Salou *et al.*, 2015) but is
432 not usually observed in classical murine EAE models (Simmons *et al.*, 2013). We also observed equivalent
433 numbers of infiltrating human T cells in the brain and the spinal cord, as opposed to the spinal cord
434 dominant pathology of most murine EAE models (Simmons *et al.*, 2013). Infiltrating T cells produced
435 predominantly Th1 and cytotoxic molecules that functioned alongside murine macrophages to
436 demyelinate the CNS. Notably, demyelination of the mouse CNS occurred without substantial
437 involvement of engrafted human macrophages, and human $CD8^+$ T cells and murine immune cells were
438 able to functionally interact ex vivo. Interspecies TCR:MHC interactions are potentially less efficient than
439 autologous antigen presentation (Halkias *et al.*, 2015), as evidenced by a relatively reduced rate of EAE
440 symptom incidence compared to classical murine EAE models (Dang *et al.*, 2015). These interactions are,
441 however, sufficient to produce demyelinating disease resulting in clinically measurable motor deficits.
442 Though a previous study incorporated myelin antigen-pulsed autologous dendritic cells (DC) to provide
443 human MHC for presentation in PBMC humanized mice (Zayoud *et al.*, 2013), our data suggest human
444 DC priming is not necessary to produce clinical EAE symptoms in HuPBMC mice. Immune system

445 reconstitution of NSG mice with human PBMCs does not precisely replicate the composition of the donor
446 PBMCs, nor all the nuanced contextual and site-specific complexities of the mammalian immune system
447 (Morillon *et al.*, 2020). Nevertheless, these data collectively demonstrate that the HuPBMC EAE model
448 is an interspecies system that exemplifies key elements of MS, and as such is a viable mouse model
449 capable of providing novel clues for causation, biomarkers, and treatment of disease.

450 PBMC donor history of EBV infection and a diagnosis of RRMS both exacerbated clinical disease
451 susceptibility and severity in HuPBMC EAE mice. Consistent with the findings of Bjornevik *et al.*, 2022,
452 clinical EAE differences could not be attributed to CMV infection status, nor to reduced serum vitamin D
453 levels. Moreover, clinical differences associated with donor EBV seropositivity in the HuPBMC EAE
454 model are consistent with findings that elevated humoral responses to EBV at disease onset are associated
455 with long-term greater disease severity and higher relapse rate in individuals with MS (Comabella *et al.*,
456 2022). Though EBV infection alone was not necessary to enable EAE development in HuPBMC mice,
457 the EBV^{+} HD recipient group presented with an intermediate phenotype that resembled RRMS recipient
458 mice in some ways more than the EBV^{-} HD group. Interestingly, active infection by EBV was not required
459 to exacerbate disease severity, as demonstrated by the absence of viral replication and memory B cell
460 responses to EBV in mice derived from donors with existing latent EBV infection. Our group has
461 previously demonstrated that viral reactivation does not occur following EAE induction in C57Bl/6 mice
462 latently infected with the murine EBV homolog, gammaherpesvirus-68 (γHV68), and that γHV68 does
463 not actively infect the CNS during EAE (Casiraghi *et al.*, 2012). B cell accumulation in the CNS of
464 HuPBMC EAE mice was also not significantly different among mice derived from donors with or without
465 EBV and RRMS. Though relatively few B cells engraft and infiltrate the CNS compared to T cells, the
466 possibility remains that engrafted B cells of varying specificities and functionalities, which can act both
467 protectively and pathogenically in classical EAE models (Rojas *et al.*, 2019; Jain and Yong, 2021), may

468 also contribute to the enhancement of disease and the increased CNS inflammation observed in EBV$^+$ and
469 RRMS recipient mice. Clinical post-mortem evidence has suggested that EBV could contribute to the
470 development and/or progression of MS through infection of CNS-infiltrating B cells and tertiary lymphoid
471 structures, leading to local inflammation (Serafini *et al.*, 2004, 2007; Pikor *et al.*, 2016). With minimal B
472 cell accumulation in the CNS at endpoint, the HuPBMC EAE model likely reflects earlier stages of MS,
473 where B cell-containing lymphoid structures have not yet formed. An important limitation of PBMC
474 humanized mice is the development of xenogeneic graft-versus-host disease, which limits the duration of
475 experiments to ~25 days post-immunization in our experience. Further investigation will be required to
476 assess the presence and influence of EBV-infected and EBV-specific B cells HuPBMC EAE mice.
477 Although there are multiple supported mechanisms by which EBV could promote an autoimmune
478 environment through B cell-specific processes, our data suggests a role for T cell immunomodulation
479 following latent infection.

480 HuPBMC EAE mice derived from EBV$^+$ HD and RRMS recipient groups had increased
481 accumulation of Th1 and cytotoxic T cells in the CNS compared to EBV$^-$ HD groups. Additionally, EBV$^+$
482 mice also had substantially reduced Treg expansion, indicating an impairment of immune regulation
483 resulting from infection. The increased abundance of effector T cells relative to regulatory T cells
484 consequently skews to promote a more inflammatory environment in mice derived from healthy donors
485 with a history of EBV infection, which further compounds when donors have also been diagnosed with
486 RRMS. Unlike in classical EAE models, where inbred mice are effectively genetically identical and highly
487 susceptible to EAE immunization (Levine and Sowinski, 1973; Marín *et al.*, 2014), the genetic variability
488 of engrafted human immune cells from unrelated donors highlights the consistency and magnitude of the
489 effect of EBV seropositivity on clinical and immunological disease outcomes in this model. Given that
490 both clinical and immunological differences were observed between the healthy donor groups differing

491 based on EBV serostatus, these effects are not entirely due to existing autoimmunity among donors. The
492 increase in infiltrating T effector cells appeared to be due to a generalized enhanced proliferative capacity
493 among T cells derived from EBV seropositive donors following TCR engagement. Further analysis will
494 be required to determine if engrafted human T cells that proliferate in the periphery express more CNS
495 homing molecules and chemokine receptors when derived from EBV^+ donors, or, if upon infiltration of
496 the CNS, EBV experienced T cells proliferate locally to a greater extent than those that are EBV naïve.
497 Regulatory T cells control effector T cell proliferation and motility in the CNS following EAE induction
498 (Koutrolos *et al.*, 2014), and thus assessment of the functional capacity of the engrafted cytotoxic T cell
499 and Treg populations would also provide insight into mechanisms by which EBV suppresses regulation
500 of effector cells following antigenic challenge.

501 As T cells are required for constant immune control of EBV-infected B cells (Long, Meckiff and
502 Taylor, 2019), latent infection could promote lasting change in predisposition to activation that may alter
503 the balance of effector and regulatory responses toward a more 'MS-like' state. In the γHV68 EAE model,
504 we also observe greater $CD8^+$ T cell infiltration of the CNS, and particularly the brain, of latently infected
505 mice, in addition to Th1-skewing, macrophage/microglia and DC activation, and reduced Treg proportions
506 in the CNS and periphery (Casiraghi *et al.*, 2012, 2015). Similar Th1-skewing and $CD8^+$ T cell
507 involvement was observed in latent γHV68-infected mice induced with rheumatoid arthritis (Mouat *et al.*,
508 2021), suggesting a common role for gammaherpesviruses in the exacerbation of and predisposition for
509 autoimmunity. Other susceptibility factors for MS, including a history of obesity, smoking and low
510 vitamin D intake, have all been suggested to act in part by promoting T cell inflammation both directly
511 and by impeding regulatory processes (Ascherio, Munger and Lünemann, 2012; Correale and Farez, 2015;
512 Fisher *et al.*, 2019; Marrodan *et al.*, 2021). Ingelfinger et al. recently identified increased CD25 expression
513 on transitional helper T cells as a defining phenotype of MS-derived PBMCs in a monozygotic twin study,

514 which the authors posit could be preferentially responsive to an environmental immune challenge such as
515 EBV infection (Ingelfinger *et al.*, 2022). Zdimerova et al. also demonstrated a synergistic interaction
516 between EBV infection and the MS risk allele HLA-DRB1*15:01 in stem cell-humanized mice, leading
517 to increased T cell reactivity to myelin antigens (Zdimerova *et al.*, 2020). Though two of four of the RRMS
518 donors who provided samples to this study expressed the HLA-DRB1*15:01 risk allele, the absence of
519 the variant among healthy donors in this small initial donor pool did not allow an analysis of the
520 downstream effects of this variant on outcomes in the HuPBMC EAE model. A focus on the interplay of
521 genetics and environmental exposures will enable more comprehensive investigation of MS risk factors
522 and targeted therapies in the HuPBMC EAE model moving forward.

523 HuPBMC mice offer the possibility of pre-screening and selecting donors based on chosen genetic
524 variants, environmental exposures, immunological conditions (Jodeleit *et al.*, 2021; Unterweger *et al.*,
525 2021), and, in the case of the HuPBMC EAE model, MS disease characteristics of interest, to create a
526 personalized immune system model. The increased brain infiltration in HuPBMC EAE mice may also aid
527 in the study of MS pathology. Though EBV induced immunomodulation of T cell responses is a possible
528 mechanism for inciting MS, it is also possible that immunomodulation occurs alongside additional virus-
529 specific mechanisms, such as infection and immortalization of autoreactive B cells, ineffective or abherent
530 immune control of EBV reactivation, and structural mimicry of CNS antigens by viral proteins (Lang *et*
531 *al.*, 2002; Pender, 2003; Laurence and Benito-León, 2017; Lanz *et al.*, 2022; Schneider-Hohendorf *et al.*,
532 2022). An important next step is to assess clinical outcomes and T cell inflammation in the model when
533 engrafted with PBMCs derived from donors with other autoimmune disorders, especially those also linked
534 to EBV infection, such as systemic lupus erythematosus and rheumatoid arthritis (Balandraud and
535 Roudier, 2018; Jog and James, 2021), to determine the generalizability of T cell immunomodulation by
536 EBV in autoimmune susceptibility. HuPBMC EAE mice could be used for directly assessing disease

537 modifying therapies specific to human immune targets, as well as indirectly by engrafting PBMCs derived
538 from patients treated with therapies such as B cell monoclonal antibodies or EBV-specific T cells (Pender
539 *et al.*, 2018). Instances of promising results from biologic testing in preclinical EAE models that translated
540 to worsened disease or serious side effects in humans could ideally also be identified in preclinical models
541 with human immune systems before advancement to clinical trials (Schmidt *et al.*, 2003; Suntharalingam
542 *et al.*, 2006; Jagessar *et al.*, 2012; Kappos *et al.*, 2014). HuPBMC mice could also be used to circumvent
543 the generation of costly transgenic mouse lines for immunogenetic studies. Furthermore, the HuPBMC
544 EAE model mechanistically reflects the epidemiological and clinical data associating EBV infection with
545 increased risk of autoimmune disease.

546 In summary, our findings highlight that EBV-mediated risk for disease in a humanized mouse
547 model of MS occurs prior to autoimmune challenge and that either the establishment or maintenance of
548 latent infection likely modulates subsequent T cell reactivity to autoantigen years later. The data support
549 prevention of EBV infection and establishment of latency as a strong avenue for MS preventative
550 strategies.

551 **MATERIALS AND METHODS**

552

553 Further information and requests for resources and reagents should be directed to and will be fulfilled by
554 the Lead Contact, Marc Horwitz (mhorwitz@mail.ubc.ca).

555

556 **Human participants**

557 Blood donation by human participants was approved by the University of British Columbia's
558 Clinical Research Ethics Board and by the Fraser Health Authority, under protocol H16-02338.
559 Individuals with RRMS were recruited at the Fraser Health MS Clinic (Burnaby, BC) under the
560 supervision of Dr. Galina Vorobeychik. Unaffected, otherwise healthy donors were recruited at the Life
561 Sciences Center (University of British Columbia). All donors were female, 19 – 39 years of age (mean
562 age 31.5 ± 6.1 years for RRMS donors and 26.4 ± 6.2 years for HDs) and provided written informed
563 consent prior to enrolment in the study, from November 2018 to August 2021. Donors with a definite
564 RRMS diagnosis, according to Poser or 2010 McDonald criteria, and disease duration of less than 10
565 years, were confirmed as treatment naïve prior to donation (no previous use of any disease modifying
566 therapies during lifetime). RRMS donors underwent a neurological exam the day of blood donation to
567 assess Expanded Disability Status Scale (EDSS) score. Individuals with a progressive MS diagnosis or
568 EDSS >4, that were male, pregnant, outside of the designated age range, or undergoing treatment were
569 excluded from the present study.

570

571 **Donor sample processing**

572 Blood samples were obtained by venipuncture and assigned an alphanumeric code to protect donor
573 identity. Whole blood (80 mL) was processed for PBMC isolation by Lymphoprep (StemCell, #07801)

574 gradient separation, according to manufacturer's instructions, within an hour of collection in K_2-EDTA
575 coated vacutainer tubes (BD, #366643). Donor PBMCs were immediately injected into recipient mice. A
576 subsample of freshly isolated PBMCs was retained for DNA isolation and flow cytometric analysis. A
577 second subsample of PBMCs was stored in autologous plasma with 10% dimethyl sufoxide and placed in
578 a Mr. Frosty™ Freezing Container (Thermo Fisher, # 5100-0001) for controlled cooling to -80°C,
579 followed by transfer to liquid nitrogen for long-term storage. Serum was obtained by centrifugation of
580 blood (15 min at 1300 x g) collected in uncoated vacutainers (BD, #367820) and frozen at -80°C prior to
581 analysis. Donor DNA samples were HLA genotyped by The Sequencing Center (Fort Collins, Colorado,
582 USA) using GenDx NGSengine® software for HLA typing (v.2.27.1).
583
584 **Animals**
585 Animal work was approved by the Animal Care Committee of the University of British Columbia,
586 under regulation of the Canadian Council of Animal Care, under protocols A17-0266 and A17-0184.
587 Adult male NSG (NOD.Cg-*Prkdc*^{scid} *Il2rg*^{tm1Wjl}/SzJ, JAX #005557), NSG-SGM3 (NOD.Cg-
588 *Prkdc*^{scid}*Il2rg*^{tm1Wjl}Tg (CMV-IL3,CSF2,KITLG)1Eav/MloySzJ, JAX #013062) and NOD (JAX #001976)
589 mice, originally sourced from the Jackson Laboratory, began experiments at 6 – 14 weeks old. In
590 preliminary experiments, we observed a greater incidence of graft-versus-host disease (GvHD) and
591 reduced EAE symptom incidence in female NSG mice compared to male NSG mice engrafted with the
592 same donor PBMCs (data not shown, DNS), and therefore male NSG mice were used as recipients for this
593 study. Moreover, NSG-SGM3 mice, which differ from the NSG by transgenic expression of human
594 hematopoietic cytokines (Nicolini *et al.*, 2004; Jangalwe *et al.*, 2016), exhibited similar incidence of EAE
595 and GvHD symptoms as NSG mice engrafted with the same donor PBMCs (DNS) and were thus used
596 interchangeably when randomized to recipient groups. Mice were bred in three facilities in Vancouver,

597 British Columbia (BC Cancer Animal Resource Centre, Centre for Disease Modelling, and Modified
598 Barrier Facility) to minimize facility-specific outcomes and housed in the same specific pathogen-free
599 facility at the University of British Columbia for the duration of experiments (Modified Barrier Facility).
600 Mice were housed in groups up to five animals per cage on corn cob bedding (Bed-o'Cobs, The
601 Andersons) and fed ad libitum with PicoLab Rodent Diet 20 (#5053) standard irradiated chow with free
602 access to autoclaved acidified water (pH 3 – 4). Housing rooms were set at 22 – 25°C with a humidity
603 range of 50 – 70%. All NSG cages were kept on the same designated immunocompromised rack on a 14.5
604 – 9.5-hour light-dark cycle with sunrise at 5:30 am, sunset at 8:00 pm.
605
606 **Humanization and EAE induction**
607 NSG mice were engrafted with 5×10^6 donor PBMCs each (or blank phosphate buffered saline
608 (PBS) for un-engrafted controls) by intravenous tail vein injection. Twelve to twenty mice per donor were
609 randomly assigned to recipient groups based on PBMC yield and available stock on the day of blood
610 donation. Following a three-week reconstitution period, circulating human $CD45^+$ cell repopulation was
611 confirmed by saphenous vein blood sampling and flow cytometric analysis. HuPBMC mice, as well as
612 un-engrafted NSG and NOD control mice for some experiments, were actively induced with EAE on day
613 0 by subcutaneous injection of a 100 µL total volume containing 200 µg MOG_{35-55} peptide (GenScript),
614 100 µg recombinant human MOG ($rhMOG_{1-120}$ prepared in-house) and 400 µg desiccated *M. Tuberculosis*
615 *H37Ra* (DIFCO, #DF3114-338) emulsified in incomplete Freund's adjuvant (DIFCO, #DF0639-60-6).
616 On days 0 and 2 post-immunization, mice received an intraperitoneal injection of 200 ng pertussis toxin
617 (List Biological Laboratories, #179A). The mice were monitored and scored daily for EAE symptoms.
618 Clinical EAE scoring was based on the following 5-point scale: 0, no overt signs of disease; 0.5, partially
619 limp tail; 1, limp tail; 1.5 limp tail and hind limb weakness; 2, loss of coordinated movements; 2.5, one

620 hind limb paralyzed; 3, both hind limbs paralyzed; 3.5, hind limbs paralyzed and weakness in forelimbs;
621 4, forelimbs paralyzed; 5, moribund state or death by EAE. Clinical outcome assessors of HuPBMC EAE
622 mice were blinded to the viral serostatus of the blood donors. Onset was defined by the occurrence of tail
623 paralysis (score 0.5 or higher) for two consecutive days. Cumulative EAE scores were calculated by
624 summing daily clinical scores from the day of onset until endpoint. Mice with motor impairments, weight
625 loss and signs of illness were provided supportive care, including administration of subcutaneous fluids
626 and cage heating, and provisions of wet food and nutritional gel. Humane endpoint was defined by an
627 EAE score of 4 or greater, or a clinical health score of 4 or greater, as defined by the Animal Care
628 Committee based on body condition, weight loss and signs of pain. Symptomatic onset of GvHD was
629 defined by the appearance and persistence or worsening of skin dryness, redness, discoloration (jaundice),
630 and/or hair loss. Due to intragroup variability in EAE symptom onset and ongoing GvHD and wasting
631 following the resolution of EAE symptoms, HuPBMC EAE mice could not be maintained longer than
632 approximately ten days post-symptom onset. Recipient cohorts were treated with the same experimental
633 interventions for humanization and EAE induction and assigned at random to different endpoint analyses.
634

635 **Recombinant human MOG protein**

636 The extracellular domain of recombinant human myelin oligodendrocyte protein ($rhMOG_{1-120}$)
637 was expressed from an *Escherichia coli* (BL21) vector (pQE-30) obtained from Drs. Christopher
638 Linington and Nancy Ruddle (Breithaupt *et al.*, 2003; Oliver, Lyon and Ruddle, 2003), and the protocol
639 was modified from that of Dr. Jennifer Gommerman. The vector expresses a 15.8 kDa His-tagged rhMOG
640 protein under the control of a lac operon. Following isopropyl ß-D-1-thiogalactopyranoside (IPTG)
641 induction, the cells were lysed to release the protein product from inclusion bodies. The protein was
642 subsequently purified using a Ni^{2+}-His-bind resin column (5 mL HisTrap FF, Cytiva, #17525501) and the

643 protein fractions were analyzed by SDS-PAGE gel electrophoresis and stained with Coomassie blue. The
644 fractions containing sufficiently pure protein of the correct molecular weight were pooled and diluted to
645 a protein concentration of <0.5 mg/mL in preparation for partial refolding in cellulose dialysis tubing (6
646 – 8 kDa molecular weight cut-off, MWCO). The refolded protein product was concentrated by
647 centrifugation in 3K MWCO Amicon tubes (EMD Millipore, #UFC900324) until a final concentration of
648 at least 4 mg/mL was reached. The final concentration was determined using a Nanodrop Lite
649 Spectrophotometer (Thermo Scientific, firmware version 1.02) (MW = 15.5 kDa, e/1000 = 12.09). Protein
650 samples were aliquoted, and flash frozen in liquid nitrogen prior to storage at -80ºC. The purified and
651 concentrated rhMOG protein was confirmed to elicit an encephalitogenic response by induction of EAE
652 symptoms in C57Bl/6 mice.
653
654 **Tissue collection**
655 Mice were euthanized at endpoint by isoflurane overdose. Blood was collected by cardiac
656 puncture, followed by perfusion with 20 mL of sterile PBS for collection of CNS tissues. Brains, spinal
657 cords, and spleens were dissected whole and kept in cold sterile PBS or in 10% neutral buffered formalin
658 (NBF) for further processing. Spinal cords were straightened, placed onto filter paper, and submerged in
659 NBF for histological analyses. The presence of intact emulsion was confirmed by examining the skin at
660 the injection site. Serum was extracted from untreated blood samples by centrifugation (13 min at 8000
661 rpm) and stored at -80°C prior to analysis. To isolate peripheral blood cells, blood samples were treated
662 with K2-EDTA for further processing. Tissues from animals in each recipient cohort were included for
663 analysis regardless of the occurrence of clinically visible EAE symptoms to account for differences in
664 incidence and severity among donor groups.
665

666 **Histological analysis**

667

668 ***Immunohistochemistry***

669 Perfused, intact organs collected for analysis of cellular infiltration by immunohistochemistry
670 (IHC) were stored in 10% NBF for 2 hours at room temperature (RT). At 2 hours, brains were halved by
671 sagittal division and incubated for another 2 hours along with the spinal cords (4 hours total in NBF at
672 RT). CNS organs were washed in cold PBS for 1 hour at 4°C to remove remaining NBF, then placed in
673 15% sucrose solution overnight at 4 °C for cryoprotection. Organs were then placed in a 30% sucrose
674 solution overnight at 4°C, then placed overnight at 4°C in a 25% sucrose solution containing 50% optimal
675 cutting temperature compound (OCT, VWR Clear Frozen Section Compound, #CA95057-838).
676 Cryoprotected organs were segmented in the case of spinal cords, and oriented in cryomolds containing
677 OCT medium and frozen on a partially submerged aluminum block equilibrated in liquid nitrogen, then
678 stored at -80°C for sectioning. Brain and spinal cord tissues were cut at -19°C into 12-µm sagittal and
679 coronal sections, respectively, using a Shandon Cryotome® FSE (Thermo), and placed onto Superfrost
680 Plus microscope slides (Fisher Scientific, #12-550-15). Sections were taken at least 30-µm apart and
681 obtained from one of either brain hemispheres, or from four equally distant points along the length of the
682 spinal cord. Sections were rehydrated in PBS for 10 min at RT, followed by blocking in 3% mouse serum
683 in PBS overnight at 4°C. Sections were thrice washed in PBS (5 min per wash) and incubated with rabbit
684 anti-human CD8 primary antibody (stock diluted 1:200 – Table M1) and/or goat anti-mouse/human Iba-
685 1 primary antibody (0.5 mg/mL stock diluted 1:300) in 3% mouse serum in PBS for 2 hours at 4°C. A rat
686 IgG isotype primary (Abcam, #ab27478) was used to confirm the specificity of the secondary antibody
687 binding to anti-human CD8. Sections were then thrice washed and incubated with AlexaFluor 680-
688 conjugated donkey anti-rabbit IgG secondary antibody (2 mg/mL stock diluted 1:600) or DyLight594-

689 conjugated mouse anti-goat IgG secondary antibody (1 mg/mL stock diluted 1:300) in 3% mouse serum
690 in PBS for 2 hours at 4°C. Sections were thrice washed with PBS then incubated for 20 min at RT in PBS
691 containing 0.2% Triton X-100 (PBT solution). CNS sections were incubated 20 min at RT in a PBT master
692 mix containing FluoroMyelin™ Green, NeuroTrace™ 530/615 and diamidino-2-phenylindole (DAPI)
693 (BrainStain™ Imaging Kit, Invitrogen #B34650). Sections were then thrice washed in PBT (15 min per
694 wash) to remove excess stain. Slides were mounted with ProLong™ Diamond Antifade Mountant medium
695 (Invitrogen, # P36961), sealed, allowed to cure for 24 hours at room temperature, and then stored at 4°C
696 until imaged.
697
698 ***Demyelination***
699 Perfused, intact spinal cords collected for analysis of myelination were stored in 10% NBF
700 overnight at RT, then moved to 70% ethanol and sent to Wax-it Histology Services Inc. for paraffin
701 embedding. To quantify myelination throughout the organ, a total of 6 – 9 consecutive 10-µm coronal
702 sections were taken from of 4 – 6 equally distanced regions along the length of the spinal cord using a
703 Shandon Finesse 325 microtome (Thermo Scientific). Sections were mounted on Superfrost Plus
704 microscope slides (Fisher Scientific, #12-550-15), dried at 37°C for one hour, and then air dried overnight
705 at RT. Sections were washed in 3 changes of xylene for 10 minutes each, then treated in 3 changes of
706 absolute ethanol for 3 minutes each and hydrated in 95% ethanol for 5 minutes. Slides were incubated in
707 eriochrome cyanine R (Sigma-Aldrich, #3564-18-9) staining solution (0.22% w/v ferric chloride, 0.5%
708 v/v sulfuric acid and 0.2% w/v eriochrome cyanine R CI 43820) for 20 minutes, run under tap water for
709 30 seconds, and incubated in differentiating solution (5.6% w/v ferric chloride) for 5 – 10 minutes until
710 only the white matter retained the stain. Slides were washed under running tap water for 5 minutes, then
711 dehydrated in 3 changes of 100% ethanol for 30 seconds each (with agitation) and cleared in 3 changes of

712 xylene for 30 seconds each (with agitation). Coverslips were mounted with VectaMount Permanent
713 Mounting Medium (Vector Laboratories, #H-5000).
714
715 ***Imaging and analysis***
716 Histology sections were imaged using a Zeiss Axio Observer 7 epi-fluorescent microscope
717 outfitted with a motorized stage (x, y, z mobility) and five LED channels. Whole organ immunofluorescent
718 sections were imaged at x20/0.65 NA air objective using an Axiocam 702 mono CMOS camera at room
719 temperature. Isotype staining was used to set LED voltages and exposures across slides per imaging
720 experiment. Immunofluorescent images were stitched and Z-stack (3 stacks of 1.2 µm each) fusion was
721 performed using a wavelet transform in Zen2.6 Pro (blue edition, Zeiss). Brightfield images of EC-stained
722 spinal cord sections were acquired at 10X/0.3 NA air objective magnification using an Axiocam 105
723 colour CMOS camera. Stitching and subsequent analysis of images was performed using Zen 2.6 Pro.
724 For EC sections, single RBG images were saved as JPEG files and quantitative analysis of staining was
725 performed using ImageJ 1.53c (NIH). Default color thresholding method was used to first select the area
726 of stained myelin and then the total area of the spinal cord. Hue, saturation, and brightness thresholds were
727 set based on fully myelinated NSG control sections and applied across all other sections. The Area
728 measurement function was used to acquire the area of the selected regions in μm^2, relative to a 200-µm
729 scale bar. Myelination was expressed as fraction of myelin-stained area of total area of the spinal cord
730 section. Replicate sections (6 – 9 consecutive sections per region) were averaged to generate 4 – 6 regional
731 myelination indices per spinal cord.
732
733
734

735 **Flow cytometric analysis**

736

737 ***Sample processing***

738 Brains, spinal cords, and spleens were kept in sterile PBS on ice, then processed into single cell
739 suspensions by passing the tissue through a 70-µm cell strainer with a syringe insert. Splenocyte
740 suspensions were incubated in red blood cell lysis buffer (150 mM NH_4Cl, 10 mM $KHCO_3$, 0.1 mM Na_2-
741 EDTA) for 10 min on ice. Whole EDTA-treated blood samples were incubated in pre-warmed red blood
742 cell lysis buffer for 15 min at RT. Brain and spinal cord samples specifically processed for the detection
743 of intracellular MBP within phagocytic cells were predigested with 0.5 mg/mL Collagenase/Dispase®
744 (Roche, #11097113001), 0.02 mg/mL DNase I (Sigma-Aldrich, #D5025) and 2% FBS in 10 mL RPMI
745 per sample for 45 min shaking at 180 rpm and 37°C. CNS cells were further isolated by resuspension in
746 40% isotonic Percoll™ solution (Cytiva, #17089101) and centrifugation (15 min at 1400 rpm) to remove
747 lipid debris. Samples analyzed for cytokine expression were incubated at 37°C (5% CO_2) for 4 hours at 1
748 – 2×10^6 splenocytes or total isolated CNS cells per 200 µL of stimulation media, containing 10% FBS, 10
749 ng/mL phorbol 12-myristate 13-acetate (PMA, Sigma-Aldrich, #P1585), 500 ng/mL ionomycin (Thermo
750 Fisher, #I24222) and 1 µL/mL GolgiPlug™ Protein Transport Inhibitor (containing Brefeldin A, BD
751 Biosciences, #555029). Cell suspensions were washed between each step with sterile PBS containing 2%
752 FBS (FACS buffer).

753

754 ***Cell sorting and co-culture***

755 For interspecies antigen presentation assays, splenocytes were isolated from EBV^+ HD PBMC-
756 engrafted male NSG mice at 4 weeks post-injection, as described above. Splenocytes were combined,
757 stained with fluorochrome-labelled anti-mCD45 and anti-hCD8 antibodies (Table M1), and positively

758 selected using a BD Influx™ cell sorter. Sorted cells were resuspended to 4×10^4 mCD45$^+$ cells with 4×10^5
759 hCD8$^+$ cells (1:10 ratio) per well in 200 µL complete culture medium (RPMI-1640 plus FBS, L-glutamine,
760 penicillin/streptomycin, MEM NEAA, sodium pyruvate, HEPES, β-mercaptoethanol), supplemented with
761 or without 20 µg/mL rhMOG protein, and incubated for 65 hours at 37°C (5% CO_2). Cells were then
762 refreshed with pre-warmed culture medium (same respective rhMOG treatments) containing 1 µL/mL
763 GolgiPlug™ Protein Transport Inhibitor and incubated for another 5 hours at 37°C (5% CO_2). Following
764 70 hours total incubation time, cells were washed with serum-free PBS and stained for flow cytometric
765 analysis as described below.
766
767 ***T cell bead stimulation assay***
768 Donor PBMC samples previously stored in autologous plasma with 10% dimethyl sulfoxide were
769 thawed from liquid nitrogen for activation analysis. Total PBMCs (5 x 10^6 cells/ mL) were stained
770 with 2.5 mM carboxyfluorescein succinimidyl ester (CFSE, Sigma #21888-25MG-F) in the dark at 4°C
771 for 8 minutes prior to quenching with newborn calf serum. An unstimulated and PMA/ionomycin-
772 stimulated subset of each sample was analyzed for baseline marker expression (PMA stimulation
773 conditions described above under 'sample processing'). Duplicate wells of 200,000 CFSE-stained cells
774 per sample were then incubated for 91 hours at 37°C (5% CO_2) at a 1:2 bead-cell ratio with Human T-
775 Activator CD3/CD28 DynaBeads™ (Thermo Fisher, #11161D) and 1 U/mL of recombinant human IL-2
776 (BioLegend, #589102) in 200 µL of complete culture medium (see above for media components). The
777 media did not contain any factors to specifically influence polarization or activation. Cells were then
778 refreshed with pre-warmed culture medium containing 1 µL/mL GolgiPlug™ Protein Transport Inhibitor
779 and incubated for another 5 hours at 37°C (5% CO_2). Following 96 hours total incubation time, cells were
780 washed with serum-free PBS and stained for flow cytometric analysis as described below.

781 ***Antibody staining and analysis***

782 Cells were stained with 1X eBioscience™ Fixable Viability Dye eFluor™ 506 (Thermo Fisher,
783 #65-0866-14) for 20 min at 4°C in serum-free PBS. Cells were then washed in FACS buffer, and
784 preincubated with human and mouse Fc block (Table M1) in FACS buffer for 10 minutes at RT. Cells
785 were washed again and incubated with fluorochrome-labelled antibodies specific to extracellular makers
786 (Table M1) in FACS buffer for 30 minutes at 4°C. Cells were washed and treated with transcription factor
787 fixation and permeabilization reagent (Thermo Fisher, #00-5521-00) for 30 min at 4°C, followed by a
788 wash with permeabilization buffer (Thermo Fisher, #00-8333-56). Cells were incubated with
789 fluorochrome-labelled antibodies specific to intracellular makers (Table M2) in permeabilization buffer
790 for 30 min at RT. Cells were washed with permeabilization and FACS buffer and resuspended in FACS
791 buffer with 2 mM EDTA for acquisition. Frozen human PBMC samples were stained as detailed above
792 for use as titration, compensation, and gating controls for all experiments. Stained cell suspensions were
793 acquired on an Attune NxT flow cytometer (Thermo Fisher) and analyzed using FlowJo™ v10.8 Software
794 (BD Life Sciences).

795

796 **Serology**

797 Endogenous antibodies to EBV, CMV and rhMOG were detected using indirect enzyme-linked
798 immunosorbent assays (ELISA). Nunc Maxisorp 96-well microtiter ELISA plates (Thermo Fisher,
799 #439454) were coated overnight at 4°C with 1 μg/well of the peptide or protein of interest (Table M3,
800 produced by ScenicBio) in 0.05 M carbonate buffer. For EBV EBNA-1 and CMV, epitope peptides 1 and
801 2 were mixed prior to well coating. The following day, the plates were washed thrice with PBS and wash
802 buffer (PBS + 0.05% Tween-20), followed by a two-hour blocking step at RT using wash buffer + 3%
803 bovine serum albumin. Plates were washed again, then incubated with serum samples serially diluted in

804 blocking buffer to generate duplicate 6-point curves (1:100 – 1:5000 for human donor serum and 1:50 –
805 1:2500 for mouse serum). After a two-hour RT incubation with serum dilutions, the plates were washed,
806 then incubated with HRP-labelled anti-human IgG antibody (Table M1) diluted 1:3000 in blocking buffer,
807 or HRP-labelled anti-human IgM diluted 1:4000, for 1 hour at 37°C. The plates were then washed with
808 PBS prior to the addition of 100 µL/well TMB substrate (BD Biosciences, #555214). Fifteen minutes after
809 the addition of substrate, 100 µL stop solution (2 N sulfuric acid) was added to each well. The plates were
810 read at 450 nm on a VarioSkan Plate Reader (Thermo Fisher) within 10 min of adding stop solution. Donor
811 serum at 1:1000 dilution was used to determine seropositivity to EBV and CMV antigens. The lower limit
812 of detection for positive IgG and IgM values was set based on the level of nonspecific background signal
813 in negative control samples (full reaction minus antigen and/or serum). Donor serum vitamin D levels
814 were quantified using a 25-OH Vitamin D ELISA assay test kit, according to the manufacturer's
815 instructions (Eagle Biosciences, #VID31-K01).
816
817 **EBV viral load**
818 Genomic DNA was isolated from a maximum of 4×10^6 donor PBMCs or mouse splenocytes per
819 sample using the PureLink™ Genomic DNA Minikit (Invitrogen, #K1820), according to the
820 manufacturer's instructions, quantified using a Nanodrop Lite Spectrophotometer (Thermo Scientific,
821 firmware version 1.02), and stored at -80°C. A *BALF5* viral DNA polymerase gene qPCR protocol adapted
822 from Kimura et al. was used to measure EBV load in DNA samples (Kimura *et al.*, 1999). The forward
823 and reverse primer and fluorogenic probe sequences are listed in Table M4 (produced by Integrated DNA
824 Technologies), along with the *BALF5* gene fragment sequence used for standard curve generation. qPCR
825 reactions comprised 300 ng genomic DNA, 0.4 µM each primer, 0.2 µM probe, and 1X QuantiNova Probe
826 PCR master mix (Qiagen, #208256). An EBV^+ B95-8 cell line extract (100 ng per reaction) was used as

827 a positive control for EBV detection. Blank water was used in negative control reactions. An 8-point
828 standard curve was generated with 1 to 10^7 *BALF5* gBlock copies per reaction. Reactions were made up
829 in Mx3000P 96-well plates (Agilent Technologies, #401333) and data were acquired using a CFX96 Real-
830 Time System C1000 Thermal Cycler (Bio-Rad) and CFX manager 3.1 software for HEX detection. The
831 cycler parameters were set according to the Qiagen QuantiNova Probe PCR protocol – 2 min at 95°C to
832 activate DNA polymerase then 45 repeats of 5 sec at 95°C and 5 sec at 60°C. Sample copies per reaction
833 were determined by interpolation of the standard curve using triplicate-averaged reaction threshold values
834 (C_T), which were then used to calculate viral load. The lower limit of detection was determined by
835 interpolating the C_T value for the lowest detectable standard point per plate and was normally ~30 EBV
836 copies/µg DNA.
837
838 **Statistical analyses**
839 Data were collated using Microsoft Excel, then graphed and statistically analyzed using GraphPad
840 Prism software 9.2.0 (GraphPad Software Inc.). Figure panels were composed in Adobe Illustrator V24.3.
841 Most graphs present group means with standard error (SEM) or standard deviation (SD) unless otherwise
842 stated in the figure legend. No statistical methods were used to predetermine sample sizes, as donor PBMC
843 yield limited recipient cohort size. No inclusion or exclusion criteria were used for analyses and groups
844 include all mice from the cohort regardless of the incidence of clinical EAE symptoms, unless otherwise
845 stated. Two normally distributed groups of data were analyzed by two-tailed, unpaired t-test with Welch's
846 correction. For three or more groups, normally distributed data were analyzed by ordinary one-way
847 analysis of variance (ANOVA) with Tukey's multiple comparisons test or Brown-Forsythe and Welch
848 ANOVA with Dunnett's T3 multiple comparisons test. If group data did not pass the Kolmogorov–
849 Smirnov normality test (or Shapiro-Wilk test when group N too small to compute KS distance), a

850 nonparametric Mann-Whitney test or Kruskal-Wallis with Dunn's multiple comparisons test was used. A
851 Log-rank (Mantel-Cox) test was used for incidence curve analysis, simple linear regression analysis for
852 cell count correlations, and ordinary two-way ANOVA for group comparisons with two variables (i.e.,
853 EAE scores over time and ELISA absorbance readings with serum dilution), where the column factor p
854 value is reported. Specific statistical tests used for each assay are noted in the figure legends, along with
855 the number of animals or replicates per group. Significance is indicated by asterisks: ****$p<0.0001$,
856 ***$p<0.001$, **$p<0.01$, and *$p<0.05$. The data that support the findings of this study are available from
857 the corresponding author upon reasonable request.
858
859 **Table M1 – Antibodies for extracellular targets**.

Target antigen	Clone	Species reactivity	Application	Source	Identifier
CD3	OKT3	Human	Flow cytometry	Thermo Fisher	56-0037-42
CD4	RPA-T4	Human	Flow cytometry	BD Biosciences	555347
CD4	RPA-T4	Human	Flow cytometry	Thermo Fisher	47-0049-42
CD8	SP16	Human	IHC-F	Thermo Fisher	MA5-14548
CD8	RPA-T8	Human	Flow cytometry	Thermo Fisher	11-0088-42
CD8	RPA-T8	Human	Flow cytometry	BD Biosciences	563821
CD11b	M1/70	Mouse	Flow cytometry	Thermo Fisher	17-0112-82
CD11c	N418	Mouse	Flow cytometry	Thermo Fisher	11-0114-85
CD14	63D3	Human	Flow cytometry	BioLegend	367142
CD14	61D3	Human	Flow cytometry	Thermo Fisher	11-0149-42
CD19	HIB19	Human	Flow cytometry	Thermo Fisher	47-0199-42
CD20	2H7	Human	Flow cytometry	BioLegend	302328
CD21	HB5	Human	Flow cytometry	Thermo Fisher	12-0219-42
CD25	CD25-4E3	Human	Flow cytometry	Thermo Fisher	11-0257-42
CD25	BC96	Human	Flow cytometry	Thermo Fisher	45-0259-42
CD27	LG.3A10	Human	Flow cytometry	BioLegend	124216
CD38	HIT2	Human	Flow cytometry	BioLegend	303529
CD40	3/23	Mouse	Flow cytometry	Thermo Fisher	MA5-17855
CD45	HI30	Human	Flow cytometry	Thermo Fisher	MHCD4517

CD45	HI30	Human	Flow cytometry	BD Biosciences	557748
CD45	30-F11	Mouse	Flow cytometry	Thermo Fisher	45-0451-82
CD45	30-F11	Mouse	Flow cytometry	Thermo Fisher	48-0451-82
CD56	TULY56	Human	Flow cytometry	Thermo Fisher	17-0566-42
CD68	Y1/82A	Human	Flow cytometry	BioLegend	333825
CD137	4B4-1	Human	Flow cytometry	BioLegend	309818
CD154 (40L)	24-31	Human	Flow cytometry	BioLegend	310823
F4/80	BM8	Mouse	Flow cytometry	Thermo Fisher	47-4801-82
Fc receptor (CD16/CD32)	2.4G2	Mouse	Flow cytometry	BD Biosciences	553142
Fc receptor	Fc1.3216	Human	Flow cytometry	BD Biosciences	564220
HLA-DR	L243	Human	Flow cytometry	Thermo Fisher	17-9952-42
Iba-1	Polyclonal	Mouse	IHC-F	Thermo Fisher	PA5-18039
IgG (H+L)	Polyclonal	Goat	IHC-F	Jackson ImmunoResearch	205-585-108
IgG (γ chain)	Polyclonal	Human	ELISA	Thermo Fisher	62-8420
IgG (H+L)	Polyclonal	Rabbit	IHC-F	Thermo Fisher	A10043
IgG2b	m2b-25G4	Mouse	Flow cytometry	Thermo Fisher	11-4220-82
IgM (μ chain)	Polyclonal	Human	ELISA	Thermo Fisher	A18841

Table M2 – Antibodies for intracellular targets.

Target antigen	Clone	Species reactivity	Application	Source	Identifier
EOMES	WD1928	Human	Flow cytometry	Thermo Fisher	11-4877-41
FOXP3	236A/E7	Human	Flow cytometry	Thermo Fisher	17-4777-42
Granzyme B	QA16A02	Human	Flow cytometry	BioLegend	372214
IFNγ	4S.B3	Human	Flow cytometry	Thermo Fisher	48-7319-42
IL-17A	eBio64DEC17	Human	Flow cytometry	Thermo Fisher	25-7179-42
Ki-67	Ki-67	Human	Flow cytometry	BioLegend	350516
MBP	MBP101	Mouse	Flow cytometry	Abcam	ab62631
RORγt	AFKJS-9	Human	Flow cytometry	Thermo Fisher	12-6988-80
T-bet	4B10	Human	Flow cytometry	Thermo Fisher	45-5825-82
TNFα	MAb11	Human	Flow cytometry	Thermo Fisher	17-7349-82

865 **Table M3 – Antigen sequences for endogenous antibody detection by ELISA**.

Antigen	Sequence
EBV VCA p18 (Liu *et al.*, 2019)	ASAGTGALASSAPSTAVAQSATPSVSSSISSLRAATSGATAAAAVDTGS GGGGQPHDTAPRGARKKQ
EBV EBNA-1 (Liu *et al.*, 2019)	Epitope 1: RSPSSQSSSSGSPPRRPPPGRRPFFHPVG
	Epitope 2: DYFEYHQEGGPDGEPDVPPGAIEQGPADDPGEGPSTGPRG
rhMOG$_{1-120}$ (Oliver, Lyon and Ruddle, 2003)	MASLSRPSLPSCLCSFLLLLLLQVSSSYAGQFRVIGPRHPIRALVGDEVE LPCRISPGKNATGMEVGWYRPPFSRVVHLYRNGKDQDGDQAPEYRG RTELLKDAIGEGKVTLRIRNVRFS
CMV (Greijer *et al.*, 1999)	Epitope 1: CETDDLDEEDTSIYLSPPPVPPVQVVAKRLPRPDTPRT
	Epitope 2: KSGTGPQPGSAGMGGAKTPSDAVQNILQKIEKIKNTEE

866

867

868 **Table M4 – DNA sequences for EBV *BALF5* qPCR assay**.

Component	Sequence (5' to 3')
Primer P1 (Kimura *et al.*, 1999)	CGGAAGCCCTCTGGACTTC
Primer P2 (Kimura *et al.*, 1999)	CCCTGTTTATCCGATGGAATG
Probe P3 (Kimura *et al.*, 1999)	/5HEX/TGTACACGC/ZEN/ACGAGAAATGCGCC/3IABkFQ/
BALF5 gene standard (gBlock)	ACC GAG ACC CGG CAG GGG GTC CTG CGG TCG AAG GTG CTG GCC TTG AGG GCG CTG AGG ACT GCA AAC TCC ACG TCC AGA CCC TGA GGC GCG CTG GCG TAG AAG TAG GCC TGC TGC CCA AAC ACG TTC ACA CAC ACG CTG GCC CCA TCG GCC TTG CGC CGG CCC AGT AGC TTG ATG ACG ATG CCA CAT GGC ACC ACA TAC CCC TGT TTA TCC GAT GGA ATG ACG GCG CAT TTC TCG TGC GTG TAC ACC GTC TCG AGT ATG TCG TAG ACA TGG AAG TCC AGA GGG CTT CCG TGG GTG TCT GCC TCC GGC CTT GCC GTG CCC TCT TGG GCA CGC TGG CGC CAC CAC ATG CCC TTT CCA TCC TCG TCA CCC CCC ACC ACC GTC AGG GAG TCT TGG TAG AAG CAC AGG GGG GGC TGA GGC CCC CGC ACA TCC ACC ACC CCT GCG GCG CCT GGT GTC TGG AAA CAC TTG GGA ATG AGAC GCA GGT ACT CCT TGT CAG GCT TTT TC

869

870 **FIGURE LEGENDS**

871

872 **Figure 1**. **Donor EBV infection and RRMS diagnosis worsen clinical outcomes in HuPBMC EAE**
873 **mice**. (A) Experimental design: Donor PBMCs isolated from women with or without a history of EBV
874 infection or an RRMS diagnosis were used to engraft immunocompromised NSG mice. Following a three-
875 week reconstitution period and confirmation of circulating human $CD45^+$ cell repopulation, humanized
876 NSG mice (HuPBMC) were immunized with recombinant human myelin oligodendrocyte glycoprotein
877 (rhMOG) antigens to induce EAE. (B) Donor serum IgG specific to acute EBV antigen viral capsid antigen
878 (VCA). (C) Donor serum IgG specific to latent EBV antigen Epstein-Barr nuclear antigen 1 (EBNA-1).
879 For B and C, group data are shown as mean with SEM and were curve fit with a one-site total binding
880 equation. Statistical differences in titre curves were assessed by ordinary two-way ANOVA. (D) Cell-
881 associated EBV viral loads in donor PBMCs. Data are shown as mean with SEM and were analyzed by
882 ordinary one-way ANOVA with Tukey's multiple comparisons test. For B – D, n = 3 – 4 donors/group
883 and the lower limit of detection (LOD) for each assay is represented by a dashed line. (E) Clinical disease
884 scores post-induction for symptomatic HuPBMC EAE mice. Data are shown as mean with SEM and
885 curves were analyzed by ordinary two-way ANOVA (n = 17 – 25 mice/group derived from 3 – 4
886 donors/group). (F) Incidence of clinical EAE symptoms post-induction. Data are shown as percentage of
887 the group and curves were analyzed by Log-rank (Mantel-Cox) test (n = 54 – 62 mice/group derived from
888 3 – 4 donors/group). (G) Day of EAE symptom onset post-induction (DPI). Distribution of individual data
889 are shown with median and quartiles (dashed lines) and were analyzed by Brown-Forsythe and Welch
890 ANOVA with Dunnett's T3 multiple comparisons test (n = 17 – 25 mice/group derived from 3 – 4
891 donors/group).

892

893 **Figure 2**. **EAE induction in HuPBMC mice causes human T cell infiltration and inflammatory**
894 **demyelination of the CNS**. (A) Demyelination of the spinal cord in the HuPBMC EAE model. Perfused
895 spinal cords were obtained days 19 – 25 post-induction (5 – 8 days post-symptom onset) from HuPBMC
896 EAE mice, and days 15 – 25 post-induction from NOD EAE mice (5 – 15 days post-symptom onset).
897 Eriochrome cyanine-stained sections (top) obtained from the lower thoracic region of the spinal cord show
898 representative myelination indices (MI) for each of the respective group means. Individual data points
899 represent averages of serial sections sampled from 4 – 6 equidistant regions along the entire length of the
900 spinal cord (n = 18 regional points from 3 unengrafted NSG control mice; n = 22 – 36 regional points
901 from 5 – 6 mice/group for EAE-induced NOD and HuPBMC groups). Distribution of individual data are
902 shown with median and quartiles (dashed lines) and were analyzed by Kruskal-Wallis with Dunn's
903 multiple comparisons test. (B – D) Human $CD8^+$ cells infiltrate the CNS of HuPBMC EAE mice engrafted
904 with RRMS donor PBMCs. Representative images of lumbar spinal cord (B) and cerebellar (C, D) sections
905 from an unengrafted control NSG mouse (left) and a symptomatic HuPBMC EAE mouse (right) derived
906 from a donor with RRMS. Perfused tissues were collected day 15 post-EAE induction (day 4 post-
907 symptom onset). Sections were labelled with FluoroMyelin (green), NeuroTrace 530/615 (red), DAPI
908 (blue), anti-hCD8 (yellow) and anti-Iba-1 (light blue). Example $hCD8^+$ cells are indicated by white arrows
909 (B, C), and $hCD8^+$ cells in proximity to Iba-1^+ cells by red arrows (D). Scale bars indicate size as specified
910 per panel, showing (A) 200 μm; (B) 200 μm, insets 50 μm; (C) 500 μm, insets 50 μm; and (D) 100 μm,
911 inset 50 μm.
912
913
914
915

916 **Figure 3**. **EAE in HuPBMC mice is mediated by infiltrating human Th1 and cytotoxic T cells and**
917 **by murine myeloid cells**. (A) Concatenated flow cytometric plots of spinal cord-infiltrating $hCD3^+CD4^+$
918 and $hCD3^+CD8^+$ T cells and their respective cytokine expression, shown as mean frequency of the parent
919 population ± SD. (B) Human T cell subsets quantified in the brain, spinal cord and spleen, shown as mean
920 with SEM. For A and B, perfused tissues were collected day 22 post-EAE induction and isolated cells
921 were stimulated with PMA and ionomycin (n = 18 mice derived from one EBV^+ HD). For C – H, perfused
922 tissues were collected days 14 – 24 post-induction of recipient cohorts derived from 2 – 3 unrelated EBV^+
923 HD PBMCs, and data were combined for analysis. (C) Human $CD8^+$:$CD4^+$ T cell ratios in the CNS and
924 spleens of HuPBMC EAE mice that either developed symptoms or remained subclinical. Data are shown
925 as mean with SEM (n = 10 – 21 mice/group) and were analyzed by Mann-Whitney test. (D) Total numbers
926 of murine $mCD45^{hi}CD11b^{hi}F4/80^+$ and human $hCD45^+CD14^+CD68^+$ macrophages in the CNS and
927 spleens of HuPBMC EAE mice. Data are shown as mean with SEM (n = 16 mice/group) and were
928 analyzed by Mann-Whitney test. (E) Frequency of murine macrophages containing intracellular myelin
929 basic protein (MBP) in HuPBMC EAE organs. Data are shown as mean with SEM (n = 16 mice/group)
930 and were analyzed by Kruskal-Wallis with Dunn's multiple comparisons test. Concatenated flow
931 cytometric plots, right, show the mean frequency of the parent population ± SD. (F) Correlation between
932 the total numbers of infiltrating $hCD3^+CD8^+$ T cells and murine macrophages containing intracellular
933 MBP in the spinal cords of HuPBMC EAE mice. Data were analyzed by simple linear regression (n = 16
934 mice). Goodness of fit is indicated by R^2 value, and the 95% confidence interval by dashed lines. (G) Total
935 numbers of infiltrating $mCD45^{hi}CD11b^{hi}F4/80^+$ macrophages in the CNS and spleens of uninduced
936 HuPBMC mice and EAE-induced HuPBMC mice that either developed symptoms or remained
937 subclinical. Data are shown as mean with SEM (n = 6 – 10 mice/group). CNS groups were analyzed by
938 Kruskal-Wallis with Dunn's multiple comparisons test and spleen groups by Brown-Forsythe and Welch

939 ANOVA with Dunnett's T3 multiple comparisons test. (H) Total numbers of murine microglia
940 (mCD45^{lo}CD11b^{hi}F4/80^{+}) containing intracellular MBP (gating scheme left) in the CNS of uninduced
941 HuPBMC mice and EAE-induced HuPBMC mice that either developed symptoms or remained
942 subclinical. Data are shown as mean with SEM (n = 6 – 10 mice/group) and were analyzed by Brown-
943 Forsythe and Welch ANOVA with Dunnett's T3 multiple comparisons test. (I) Interspecies co-culture
944 assay design: NSG mice (n = 4) were engrafted with PBMC from an EBV^{+} HD, and after four weeks,
945 reconstituted spleens were processed and combined for fluorescence-activated cell sorting (FACS). Sorted
946 cells were cultured 1 mCD45^{+}:10 hCD8^{+} cells per well in blank or rhMOG-supplemented complete culture
947 medium for 70 hours. (J) Changes in mCD11c^{+} and hCD8^{+} cell marker expression following myelin
948 antigen exposure in culture. Data are shown as mean with SEM (n = 5 replicate wells/group) and analyzed
949 by Mann-Whitney test (mCD11c^{+} data) or by unpaired t-test with Welch's correction (hCD8^{+} data).
950 Median fluorescence intensity (MFI).
951
952 **Figure 4**. **Donor EBV and RRMS status promote human immune cell infiltration of the HuPBMC**
953 **EAE CNS without viral reactivation**. (A) Total human CD45^{+} immune cell counts, (B) hCD19^{+} B cell
954 counts, (C) hCD3^{+} T cell counts, (D) EBV genome copies in splenic DNA, (E) hCD3^{+}CD4^{+} T cell counts
955 and (F) hCD3^{+}CD8^{+} T cell counts in the brain, spinal cord, and spleen of recipient HuPBMC EAE mice
956 at endpoint, grouped by PBMC donor EBV serostatus and RRMS diagnosis. Perfused organs were
957 collected days 14 – 27 post-EAE induction (average 5 – 10 days post-symptom onset). For total immune
958 cell quantification, n = 29 – 35 mice/group derived from 2 – 3 donors/group. For viral load quantification,
959 n = 28 – 53 mice/group derived from 2 – 4 blood donors/group; n = 5 replicates for control EBV^{+} B95-8
960 cell line and assay lower limit of detection is represented by a dashed line. All data are shown as mean
961 with SEM and were analyzed by Kruskal-Wallis with Dunn's multiple comparisons test.

962 **Figure 5**. **Donor EBV and RRMS status promote effector T cell expansion in the HuPBMC EAE**
963 **model**. Figure shows brain and spinal cord infiltration and spleen reconstitution in recipient HuPBMC
964 EAE mice at endpoint, grouped by PBMC donor EBV serostatus and RRMS diagnosis. (A) Concatenated
965 flow cytometric plots of IFNγ and IL-17A expression, showing the mean frequency of $hCD3^+CD4^+$ cells
966 ± SD, as well as corresponding total (B) $IFN\gamma^+(IL\text{-}17A^-)$, (C) $IL\text{-}17A^+(IFN\gamma^-)$, and (D) $IFN\gamma^+IL\text{-}17A^+$
967 $hCD4^+$ T cell counts in each tissue. (E) Concatenated flow cytometric plots of IFNγ and GzmB expression,
968 showing the mean frequency of $hCD3^+CD8^+$ cells ± SD, quantified as (F) $\%IFN\gamma^+(GzmB^-)$, (G)
969 $\%GzmB^+(IFN\gamma^-)$, and (H) $\%IFN\gamma^+GzmB^+$ of $hCD3^+CD8^+$ cells in each tissue. Perfused organs were
970 collected days 14 – 27 post-EAE induction (average 5 – 10 days post-symptom onset). Isolated immune
971 cells were stimulated with PMA and ionomycin for cytokine detection (n = 9 – 20 mice/group derived
972 from 1 – 2 donors/group). All plotted data are shown as mean with SEM and were analyzed by Brown-
973 Forsythe and Welch ANOVA with Dunnett's T3 multiple comparisons test or by Kruskal-Wallis with
974 Dunn's multiple comparisons test.
975
976 **Figure 6**. **Donor EBV and RRMS status limit regulatory T cell expansion in HuPBMC EAE mice**.
977 The proportion of $hCD3^+CD4^+$ T cells expressing FOXP3 in (A) freshly isolated donor PBMC (n = 3 – 4
978 donors/group), (B) in the peripheral blood of engrafted HuPBMC mice at 3 weeks post-PBMC injection
979 (n = 57 – 62 mice/group derived from 3 – 4 donors/group), and in the (C) brain, (D) spinal cord, and (E)
980 spleen of HuPBMC EAE mice at endpoint (n = 30 – 35 mice/group derived from 2 – 3 donors/group). The
981 ratio of infiltrating (F) $hCD4^+IFN\gamma^+$ (Th1) and (G) $hCD8^+IFN\gamma^+GzmB^+$ (Tc) to regulatory $hCD4^+FOXP3^+$
982 (Treg) cells per tissue in recipient HuPBMC EAE mice at endpoint, grouped by PBMC donor EBV
983 serostatus and RRMS diagnosis (n = 7 – 20 mice/group from 1 – 2 donors/group). Cells were isolated
984 from perfused organs collected days 14 – 27 post-EAE induction (average 5 – 10 days post-symptom

985 onset) and, for cytokine detection, stimulated with PMA and ionomycin. Data are shown as mean with
986 SEM and were analyzed by Brown-Forsythe and Welch ANOVA with Dunnett's T3 multiple comparisons
987 test (A) or by Kruskal-Wallis with Dunn's multiple comparisons test (B – G).
988
989 **Figure 7**. **Donor T cell proliferation is enhanced by both EBV seropositivity and RRMS**. Previously
990 frozen, whole PBMC samples from EBV^+ RRMS, EBV^+ HD, and EBV^- HD blood donors were incubated
991 with anti-CD3/CD28 coated beads for 96 hours to stimulate T cells in the absence of specific antigen.
992 Figure shows (A) the proliferation index determined by CFSE staining, (B) the proportion of $hCD4^+$ T
993 cells having undergone a specified number of cellular divisions by CFSE staining, (C) Ki-67 expression,
994 (D) TNFα expression and (E) IFNγ and IL-17A expression on $hCD3^+CD4^+$ T cells, as well as, (F) the
995 proliferation index determined by CFSE staining, (G) the proportion of $hCD8^+$ T cells having undergone
996 a specified number of cellular divisions by CFSE staining, (H) Ki-67 expression, (I) TNFα expression
997 and (J) IFNγ expression on $hCD3^+CD8^+$ T cells. Concatenated flow plots indicate the sum proportion of
998 marker positive cells for all donors in each group. The colored symbol legend is applicable to all
999 comparisons (n = 3 – 4 blood donors/group). All plotted data are shown as mean with SEM and were
000 analyzed by Brown-Forsythe and Welch ANOVA with Dunnett's T3 multiple comparisons test or by
001 Kruskal-Wallis with Dunn's multiple comparisons test.
002
003
004
005
006
007

008 **TABLE LEGENDS**

009

010 **Table 1**. **PBMC donor demographics, disease characteristics, and serology**. All RRMS and healthy
011 donors were female. RRMS participants were treatment naïve and in clinical remission at the time of
012 donation. Abbreviations: Healthy donor, HD; Expanded Disability Status Scale, EDSS; Viral capsid
013 antigen, VCA; Epstein-Barr nuclear antigen 1, EBNA-1; Cytomegalovirus, CMV.

014 **REFERENCES**

015

016 Abrahamyan, S. *et al.* (2020) 'Complete Epstein-Barr virus seropositivity in a large cohort of patients with
017 early multiple sclerosis', *Journal of Neurology, Neurosurgery & Psychiatry*, 91(7), pp. 681–686.
018 Available at: https://doi.org/10.1136/jnnp-2020-322941.

019 Alotaibi, S. *et al.* (2004) 'Epstein-Barr virus in pediatric multiple sclerosis', *JAMA*, 291(15), pp. 1875–
020 1879. Available at: https://doi.org/10.1001/jama.291.15.1875.

021 Ascherio *et al.* (2001) 'Epstein-barr virus antibodies and risk of multiple sclerosis: A prospective study',
022 *JAMA*, 286(24), pp. 3083–3088. Available at: https://doi.org/10.1001/jama.286.24.3083.

023 Ascherio, A., Munger, K.L. and Lünemann, J.D. (2012) 'The initiation and prevention of multiple
024 sclerosis', *Nature Reviews Neurology*, 8(11), pp. 602–612. Available at:
025 https://doi.org/10.1038/nrneurol.2012.198.

026 Babbe, H. *et al.* (2000) 'Clonal Expansions of Cd8+ T Cells Dominate the T Cell Infiltrate in Active
027 Multiple Sclerosis Lesions as Shown by Micromanipulation and Single Cell Polymerase Chain Reaction',
028 *The Journal of Experimental Medicine*, 192(3), pp. 393–404.

029 Baker, D. *et al.* (2019) 'Autoimmune encephalomyelitis in NOD mice is not initially a progressive
030 multiple sclerosis model', *Annals of Clinical and Translational Neurology*, 6(8), pp. 1362–1372.
031 Available at: https://doi.org/10.1002/acn3.792.

032 Balandraud, N. and Roudier, J. (2018) 'Epstein-Barr virus and rheumatoid arthritis', *Joint Bone Spine*,
033 85(2), pp. 165–170. Available at: https://doi.org/10.1016/j.jbspin.2017.04.011.

034 Balfour, H.H., Jr *et al.* (2013) 'Age-Specific Prevalence of Epstein–Barr Virus Infection Among
035 Individuals Aged 6–19 Years in the United States and Factors Affecting Its Acquisition', *The Journal of*
036 *Infectious Diseases*, 208(8), pp. 1286–1293. Available at: https://doi.org/10.1093/infdis/jit321.

037 Banwell, B. *et al.* (2007) 'Clinical features and viral serologies in children with multiple sclerosis: a
038 multinational observational study', *The Lancet Neurology*, 6(9), pp. 773–781. Available at:
039 https://doi.org/10.1016/S1474-4422(07)70196-5.

040 Bar-Or, A. *et al.* (2020) 'Epstein–Barr Virus in Multiple Sclerosis: Theory and Emerging
041 Immunotherapies', *Trends in Molecular Medicine*, 26(3), pp. 296–310. Available at:
042 https://doi.org/10.1016/j.molmed.2019.11.003.

043 Bitsch, A. *et al.* (2000) 'Acute axonal injury in multiple sclerosis: Correlation with demyelination and
044 inflammation', *Brain*, 123(6), pp. 1174–1183. Available at: https://doi.org/10.1093/brain/123.6.1174.

045 Bjornevik, K. *et al.* (2022) 'Longitudinal analysis reveals high prevalence of Epstein-Barr virus associated
046 with multiple sclerosis', *Science* [Preprint]. Available at:
047 https://www.science.org/doi/abs/10.1126/science.abj8222 (Accessed: 13 January 2022).

048 Breithaupt, C. *et al.* (2003) 'Structural insights into the antigenicity of myelin oligodendrocyte
049 glycoprotein', *Proceedings of the National Academy of Sciences of the United States of America*, 100(16),
050 pp. 9446–9451. Available at: https://doi.org/10.1073/pnas.1133443100.

051 Casiraghi, C. *et al.* (2012) 'Gammaherpesvirus Latency Accentuates EAE Pathogenesis: Relevance to
052 Epstein-Barr Virus and Multiple Sclerosis', *PLoS Pathogens*, 8(5). Available at:
053 https://doi.org/10.1371/journal.ppat.1002715.

054 Casiraghi, C. *et al.* (2015) 'Latent virus infection upregulates CD40 expression facilitating enhanced
055 autoimmunity in a model of multiple sclerosis', *Scientific Reports*, 5, p. 13995. Available at:
056 https://doi.org/10.1038/srep13995.

057 Chaganti, S. *et al.* (2009) 'Epstein-Barr virus colonization of tonsillar and peripheral blood B-cell subsets
058 in primary infection and persistence', *Blood*, 113(25), pp. 6372–6381. Available at:
059 https://doi.org/10.1182/blood-2008-08-175828.

060 Chen, M.-R. (2011) 'Epstein–Barr Virus, the Immune System, and Associated Diseases', *Frontiers in*
061 *Microbiology*, 2, p. 5. Available at: https://doi.org/10.3389/fmicb.2011.00005.

062 Chen, Y. *et al.* (2022) 'Environmental Factors for Epstein-Barr Virus Reactivation in a High-Risk Area
063 of Nasopharyngeal Carcinoma: A Population-Based Study', *Open Forum Infectious Diseases*, 9(5), p.
064 ofac128. Available at: https://doi.org/10.1093/ofid/ofac128.

065 Comabella, M. *et al.* (2022) 'Increased cytomegalovirus immune responses at disease onset are protective
066 in the long-term prognosis of patients with multiple sclerosis', *Journal of Neurology, Neurosurgery, and*
067 *Psychiatry*, p. jnnp-2022-330205. Available at: https://doi.org/10.1136/jnnp-2022-330205.

068 Compston, A. and Coles, A. (2008) 'Multiple sclerosis', *The Lancet*, 372(9648), pp. 1502–1517. Available
069 at: https://doi.org/10.1016/S0140-6736(08)61620-7.

070 Correale, J. and Farez, M.F. (2015) 'Smoking worsens multiple sclerosis prognosis: Two different
071 pathways are involved', *Journal of Neuroimmunology*, 281, pp. 23–34. Available at:
072 https://doi.org/10.1016/j.jneuroim.2015.03.006.

073 Dang, P.T. *et al.* (2015) 'Modelling MS: Chronic-Relapsing EAE in the NOD/Lt Mouse Strain', in A.C.
074 La Flamme and Jacqueline Monique Orian (eds) *Emerging and Evolving Topics in Multiple Sclerosis*
075 *Pathogenesis and Treatments*. Cham: Springer International Publishing (Current Topics in Behavioral
076 Neurosciences), pp. 143–177. Available at: https://doi.org/10.1007/7854_2015_378.

077 DeLorenze *et al.* (2006) 'Epstein-barr virus and multiple sclerosis: Evidence of association from a
078 prospective study with long-term follow-up', *Archives of Neurology*, 63(6), pp. 839–844. Available at:
079 https://doi.org/10.1001/archneur.63.6.noc50328.

080 Dendrou, C.A., Fugger, L. and Friese, M.A. (2015) 'Immunopathology of multiple sclerosis', *Nature*
081 *Reviews Immunology*, 15(9), pp. 545–558. Available at: https://doi.org/10.1038/nri3871.

082 Dong, Y. and Yong, V.W. (2019) 'When encephalitogenic T cells collaborate with microglia in multiple
083 sclerosis', *Nature Reviews Neurology*, 15(12), pp. 704–717. Available at: https://doi.org/10.1038/s41582-
084 019-0253-6.

085 Dunmire, S.K., Hogquist, K.A. and Balfour, H.H. (2015) 'Infectious Mononucleosis', *Current topics in*
086 *microbiology and immunology*, 390, pp. 211–240. Available at: https://doi.org/10.1007/978-3-319-22822-
087 8_9.

088 Fisher, S.A. *et al.* (2019) 'The role of vitamin D in increasing circulating T regulatory cell numbers and
089 modulating T regulatory cell phenotypes in patients with inflammatory disease or in healthy volunteers:
090 A systematic review', *PLoS ONE*, 14(9), p. e0222313. Available at:
091 https://doi.org/10.1371/journal.pone.0222313.

092 Furtado, G.C. *et al.* (2008) 'Swift Entry of Myelin-Specific T Lymphocytes into the Central Nervous
093 System in Spontaneous Autoimmune Encephalomyelitis', *Journal of immunology (Baltimore, Md. :*
094 *1950)*, 181(7), pp. 4648–4655.

095 Gasper-Smith, N., Marriott, I. and Bost, K.L. (2006) 'Murine γ-Herpesvirus 68 Limits Naturally Occurring
096 CD4+CD25+ T Regulatory Cell Activity following Infection', *The Journal of Immunology*, 177(7), pp.
097 4670–4678. Available at: https://doi.org/10.4049/jimmunol.177.7.4670.

098 Gorantla, S., Gendelman, H.E. and Poluektova, L.Y. (2012) 'Can Humanized Mice Reflect the Complex
099 Pathobiology of HIV-Associated Neurocognitive Disorders?', *Journal of neuroimmune pharmacology :*
100 *the official journal of the Society on NeuroImmune Pharmacology*, 7(2), pp. 352–362. Available at:
101 https://doi.org/10.1007/s11481-011-9335-y.

102 Greijer, A.E. *et al.* (1999) 'Molecular Fine-Specificity Analysis of Antibody Responses to Human
103 Cytomegalovirus and Design of Novel Synthetic-Peptide-Based Serodiagnostic Assays', *Journal of*
104 *Clinical Microbiology* [Preprint]. Available at: https://doi.org/10.1128/JCM.37.1.179-188.1999.

105 Hadinoto, V. *et al.* (2008) 'On the dynamics of acute EBV infection and the pathogenesis of infectious
106 mononucleosis', *Blood*, 111(3), pp. 1420–1427. Available at: https://doi.org/10.1182/blood-2007-06-
107 093278.

108 Halkias, J. *et al.* (2015) 'Conserved and divergent aspects of human T-cell development and migration in
109 humanized mice', *Immunology and Cell Biology*, 93(8), pp. 716–726. Available at:
110 https://doi.org/10.1038/icb.2015.38.

111 Handel, A.E. *et al.* (2010) 'An Updated Meta-Analysis of Risk of Multiple Sclerosis following Infectious
112 Mononucleosis', *PLoS ONE*, 5(9), p. e12496. Available at: https://doi.org/10.1371/journal.pone.0012496.

113 Heuts, F. *et al.* (2014) 'T Cells Modulate Epstein-Barr Virus Latency Phenotypes during Infection of
114 Humanized Mice', *Journal of Virology*, 88(6), pp. 3235–3245. Available at:
115 https://doi.org/10.1128/JVI.02885-13.

116 Hjalgrim, H., Friborg, J. and Melbye, M. (2007) 'The epidemiology of EBV and its association with
117 malignant disease', in A. Arvin et al. (eds) *Human Herpesviruses: Biology, Therapy, and*
118 *Immunoprophylaxis*. Cambridge: Cambridge University Press. Available at:
119 http://www.ncbi.nlm.nih.gov/books/NBK47424/ (Accessed: 28 January 2022).

120 Hohlfeld, R. and Steinman, L. (2017) 'T Cell–Transfer Experimental Autoimmune Encephalomyelitis:
121 Pillar of Multiple Sclerosis and Autoimmunity', *The Journal of Immunology*, 198(9), pp. 3381–3383.
122 Available at: https://doi.org/10.4049/jimmunol.1700346.

123 Houldcroft, C.J. and Kellam, P. (2015) 'Host genetics of Epstein–Barr virus infection, latency and
124 disease', *Reviews in Medical Virology*, 25(2), pp. 71–84. Available at: https://doi.org/10.1002/rmv.1816.

125 Ingelfinger, F. *et al.* (2022) 'Twin study reveals non-heritable immune perturbations in multiple sclerosis',
126 *Nature*, pp. 1–7. Available at: https://doi.org/10.1038/s41586-022-04419-4.

127 Islas-Ohlmayer, M. *et al.* (2004) 'Experimental Infection of NOD/SCID Mice Reconstituted with Human
128 CD34+ Cells with Epstein-Barr Virus', *Journal of Virology*, 78(24), pp. 13891–13900. Available at:
129 https://doi.org/10.1128/JVI.78.24.13891-13900.2004.

130 Jagessar, S.A. *et al.* (2012) 'Antibodies Against Human BLyS and APRIL Attenuate EAE Development
131 in Marmoset Monkeys', *Journal of Neuroimmune Pharmacology*, 7(3), pp. 557–570. Available at:
132 https://doi.org/10.1007/s11481-012-9384-x.

133 Jagessar, S.A. *et al.* (2013) 'The Different Clinical Effects of Anti-BLyS, Anti-APRIL and Anti-CD20
134 Antibodies Point at a Critical Pathogenic Role of γ-Herpesvirus Infected B Cells in the Marmoset EAE
135 Model', *Journal of Neuroimmune Pharmacology*, 8(3), pp. 727–738. Available at:
136 https://doi.org/10.1007/s11481-013-9448-6.

137 Jain, R.W. and Yong, V.W. (2021) 'B cells in central nervous system disease: diversity, locations and
138 pathophysiology', *Nature Reviews. Immunology*, pp. 1–12. Available at: https://doi.org/10.1038/s41577-
139 021-00652-6.

140 Jangalwe, S. *et al.* (2016) 'Improved B cell development in humanized NOD-scid IL2Rγnull mice
141 transgenically expressing human stem cell factor, granulocyte-macrophage colony-stimulating factor and
142 interleukin-3', *Immunity, Inflammation and Disease*, 4(4), pp. 427–440. Available at:
143 https://doi.org/10.1002/iid3.124.

144 Jodeleit, H. *et al.* (2021) 'Head-to-head study of oxelumab and adalimumab in a mouse model of ulcerative
145 colitis based on NOD/Scid IL2Rγnull mice reconstituted with human peripheral blood mononuclear cells',
146 *Disease Models & Mechanisms*, 14(1), p. dmm046995. Available at:
147 https://doi.org/10.1242/dmm.046995.

148 Jog, N.R. and James, J.A. (2021) 'Epstein Barr Virus and Autoimmune Responses in Systemic Lupus
149 Erythematosus', *Frontiers in Immunology*, 11. Available at:
150 https://www.frontiersin.org/articles/10.3389/fimmu.2020.623944 (Accessed: 7 December 2022).

151 Kappos, L. *et al.* (2014) 'Atacicept in multiple sclerosis (ATAMS): a randomised, placebo-controlled,
152 double-blind, phase 2 trial', *The Lancet Neurology*, 13(4), pp. 353–363. Available at:
153 https://doi.org/10.1016/S1474-4422(14)70028-6.

154 Kimura, H. *et al.* (1999) 'Quantitative Analysis of Epstein-Barr Virus Load by Using a Real-Time PCR
155 Assay', *Journal of Clinical Microbiology*, 37(1), pp. 132–136.

156 Klineova, S. and Lublin, F.D. (2018) 'Clinical Course of Multiple Sclerosis', *Cold Spring Harbor*
157 *Perspectives in Medicine*, 8(9), p. a028928. Available at: https://doi.org/10.1101/cshperspect.a028928.

158 Koutrolos, M. *et al.* (2014) 'Treg cells mediate recovery from EAE by controlling effector T cell
159 proliferation and motility in the CNS', *Acta Neuropathologica Communications*, 2(1), p. 163. Available
160 at: https://doi.org/10.1186/s40478-014-0163-1.

161 Kroger, C.J. and Alexander-Miller, M.A. (2007) 'Dose-dependent modulation of CD8 and functional
162 avidity as a result of peptide encounter', *Immunology*, 122(2), pp. 167–178. Available at:
163 https://doi.org/10.1111/j.1365-2567.2007.02622.x.

164 Kuwana, Y. *et al.* (2011) 'Epstein-Barr Virus Induces Erosive Arthritis in Humanized Mice', *PLoS ONE*,
165 6(10). Available at: https://doi.org/10.1371/journal.pone.0026630.

166 Lachmann, R. *et al.* (2018) 'Cytomegalovirus (CMV) seroprevalence in the adult population of Germany',
167 *PLOS ONE*, 13(7), p. e0200267. Available at: https://doi.org/10.1371/journal.pone.0200267.

168 Lang, H.L.E. *et al.* (2002) 'A functional and structural basis for TCR cross-reactivity in multiple sclerosis',
169 *Nature Immunology*, 3(10), pp. 940–943. Available at: https://doi.org/10.1038/ni835.

170 Lang, J. *et al.* (2017) 'Replacing mouse BAFF with human BAFF does not improve B-cell maturation in
171 hematopoietic humanized mice', *Blood Advances*, 1(27), pp. 2729–2741. Available at:
172 https://doi.org/10.1182/bloodadvances.2017010090.

173 Lanz, T.V. *et al.* (2022) 'Clonally Expanded B Cells in Multiple Sclerosis Bind EBV EBNA1 and
174 GlialCAM', *Nature*, pp. 1–12. Available at: https://doi.org/10.1038/s41586-022-04432-7.

175 Laurence, M. and Benito-León, J. (2017) 'Epstein–Barr virus and multiple sclerosis: Updating Pender's
176 hypothesis', *Multiple Sclerosis and Related Disorders*, 16, pp. 8–14. Available at:
177 https://doi.org/10.1016/j.msard.2017.05.009.

178 Levin, L.I. *et al.* (2010) 'Primary Infection with the Epstein-Barr Virus and Risk of Multiple Sclerosis',
179 *Annals of neurology*, 67(6), pp. 824–830. Available at: https://doi.org/10.1002/ana.21978.

180 Levine, S. and Sowinski, R. (1973) 'Experimental Allergic Encephalomyelitis in Inbred and Outbred
181 Mice', *The Journal of Immunology*, 110(1), pp. 139–143. Available at:
182 https://doi.org/10.4049/jimmunol.110.1.139.

183 Lim, W.H. *et al.* (2007) 'Human plasmacytoid dendritic cells regulate immune responses to Epstein-Barr
184 virus (EBV) infection and delay EBV-related mortality in humanized NOD-SCID mice', *Blood*, 109(3),
185 pp. 1043–1050. Available at: https://doi.org/10.1182/blood-2005-12-024802.

186 Lin, X. *et al.* (2015) 'The Epstein-Barr Virus BART miRNA Cluster of the M81 Strain Modulates Multiple
187 Functions in Primary B Cells', *PLoS Pathogens*, 11(12). Available at:
188 https://doi.org/10.1371/journal.ppat.1005344.

189 Liu, Z. *et al.* (2019) 'Multilaboratory Assessment of Epstein-Barr Virus Serologic Assays: the Case for
190 Standardization', *Journal of Clinical Microbiology*, 57(11), pp. e01107-19. Available at:
191 https://doi.org/10.1128/JCM.01107-19.

192 Long, H.M., Meckiff, B.J. and Taylor, G.S. (2019) 'The T-cell Response to Epstein-Barr Virus–New
193 Tricks From an Old Dog', *Frontiers in Immunology*, 10, p. 2193. Available at:
194 https://doi.org/10.3389/fimmu.2019.02193.

195 Lünemann, J.D. *et al.* (2006) 'Increased frequency and broadened specificity of latent EBV nuclear
196 antigen-1-specific T cells in multiple sclerosis', *Brain: A Journal of Neurology*, 129(Pt 6), pp. 1493–1506.
197 Available at: https://doi.org/10.1093/brain/awl067.

198 Lünemann, J.D. *et al.* (2008) 'EBNA1-specific T cells from patients with multiple sclerosis cross react
199 with myelin antigens and co-produce IFN-γ and IL-2', *The Journal of Experimental Medicine*, 205(8), pp.
200 1763–1773. Available at: https://doi.org/10.1084/jem.20072397.

201 Marín, N. *et al.* (2014) 'Regulatory Lymphocytes Are Key Factors in MHC-Independent Resistance to
202 EAE', *Journal of Immunology Research*, 2014, p. e156380. Available at:
203 https://doi.org/10.1155/2014/156380.

204 Marrodan, M. *et al.* (2021) 'Obesity and the risk of Multiple Sclerosis. The role of Leptin', *Annals of*
205 *Clinical and Translational Neurology*, 8(2), pp. 406–424. Available at:
206 https://doi.org/10.1002/acn3.51291.

207 McKay, K.A. *et al.* (2016) 'Factors associated with onset, relapses or progression in multiple sclerosis: A
208 systematic review', *NeuroToxicology* [Preprint]. Available at:
209 https://doi.org/10.1016/j.neuro.2016.03.020.

210 Melkus, M.W. *et al.* (2006) 'Humanized mice mount specific adaptive and innate immune responses to
211 EBV and TSST-1', *Nature Medicine*, 12(11), pp. 1316–1322. Available at:
212 https://doi.org/10.1038/nm1431.

213 Miller, S.D., Karpus, W.J. and Davidson, T.S. (2007) 'Experimental Autoimmune Encephalomyelitis in
214 the Mouse', *Current protocols in immunology / edited by John E. Coligan ... [et al.]*, CHAPTER, p. Unit-
215 15.1. Available at: https://doi.org/10.1002/0471142735.im1501s77.

216 Morillon, Y.M. *et al.* (2020) 'The Development of Next-generation PBMC Humanized Mice for
217 Preclinical Investigation of Cancer Immunotherapeutic Agents', *Anticancer Research*, 40(10), pp. 5329–
218 5341. Available at: https://doi.org/10.21873/anticanres.14540.

219 Mouat, I.C. *et al.* (2021) 'Latent gammaherpesvirus exacerbates arthritis through modification of age-
220 associated B cells', *eLife*, 10, p. e67024. Available at: https://doi.org/10.7554/eLife.67024.

221 Mouhieddine, T.H. *et al.* (2015) 'Risk factors for multiple sclerosis and associations with anti-EBV
222 antibody titers', *Clinical Immunology*, 158(1), pp. 59–66. Available at:
223 https://doi.org/10.1016/j.clim.2015.03.011.

224 Münz, C. (2015) 'EBV Infection of Mice with Reconstituted Human Immune System Components', in C.
225 Münz (ed.) *Epstein Barr Virus Volume 2*. Springer International Publishing (Current Topics in
226 Microbiology and Immunology, 391), pp. 407–423. Available at: https://doi.org/10.1007/978-3-319-
227 22834-1_14.

228 Nicolini, F.E. *et al.* (2004) 'NOD/SCID mice engineered to express human IL-3, GM-CSF and Steel factor
229 constitutively mobilize engrafted human progenitors and compromise human stem cell regeneration',
230 *Leukemia*, 18(2), pp. 341–347. Available at: https://doi.org/10.1038/sj.leu.2403222.

231 Olivadoti, M. *et al.* (2007) 'Murine Gammaherpesvirus 68: A Model for the Study of Epstein-Barr Virus
232 Infections and Related Diseases', *Comparative Medicine*, 57(1), pp. 44–50.

233 Oliver, A.R., Lyon, G.M. and Ruddle, N.H. (2003) 'Rat and Human Myelin Oligodendrocyte
234 Glycoproteins Induce Experimental Autoimmune Encephalomyelitis by Different Mechanisms in
235 C57BL/6 Mice', *The Journal of Immunology*, 171(1), pp. 462–468. Available at:
236 https://doi.org/10.4049/jimmunol.171.1.462.

237 Olsson, T., Barcellos, L.F. and Alfredsson, L. (2017) 'Interactions between genetic, lifestyle and
238 environmental risk factors for multiple sclerosis', *Nature Reviews. Neurology*, 13(1), pp. 25–36. Available
239 at: https://doi.org/10.1038/nrneurol.2016.187.

240 Pender, M.P. (2003) 'Infection of autoreactive B lymphocytes with EBV, causing chronic autoimmune
241 diseases', *Trends in Immunology*, 24(11), pp. 584–588. Available at:
242 https://doi.org/10.1016/j.it.2003.09.005.

243 Pender, M.P. *et al.* (2018) 'Epstein-Barr virus–specific T cell therapy for progressive multiple sclerosis',
244 *JCI Insight*, 3(22), p. e124714. Available at: https://doi.org/10.1172/jci.insight.124714.

245 Pikor, N.B. *et al.* (2016) 'Meningeal Tertiary Lymphoid Tissues and Multiple Sclerosis: A Gathering
246 Place for Diverse Types of Immune Cells during CNS Autoimmunity', *Frontiers in Immunology*, 6.
247 Available at: https://doi.org/10.3389/fimmu.2015.00657.

248 Pratt, Z.L., Zhang, J. and Sugden, B. (2012) 'The Latent Membrane Protein 1 (LMP1) Oncogene of
249 Epstein-Barr Virus Can Simultaneously Induce and Inhibit Apoptosis in B Cells', *Journal of Virology*,
250 86(8), pp. 4380–4393. Available at: https://doi.org/10.1128/JVI.06966-11.

251 Quan, T.E. *et al.* (2010) 'Epstein-Barr Virus Promotes Interferon-α Production by Plasmacytoid Dendritic
252 Cells', *Arthritis and rheumatism*, 62(6), pp. 1693–1701. Available at: https://doi.org/10.1002/art.27408.

253 Rojas, O.L. *et al.* (2019) 'Recirculating Intestinal IgA-Producing Cells Regulate Neuroinflammation via
254 IL-10', *Cell*, 176(3), pp. 610-624.e18. Available at: https://doi.org/10.1016/j.cell.2018.11.035.

255 Rommer, P.S. *et al.* (2020) 'Relapsing and progressive MS: the sex-specific perspective', *Therapeutic*
256 *Advances in Neurological Disorders*, 13, p. 1756286420956495. Available at:
257 https://doi.org/10.1177/1756286420956495.

258 Sallah, N. *et al.* (2020) 'Distinct genetic architectures and environmental factors associate with host
259 response to the γ2-herpesvirus infections', *Nature Communications*, 11(1), p. 3849. Available at:
260 https://doi.org/10.1038/s41467-020-17696-2.

261 Salou, M. *et al.* (2015) 'Expanded CD8 T-cell sharing between periphery and CNS in multiple sclerosis',
262 *Annals of Clinical and Translational Neurology*, 2(6), pp. 609–622. Available at:
263 https://doi.org/10.1002/acn3.199.

264 Sato, K. *et al.* (2011) 'A novel animal model of Epstein-Barr virus–associated hemophagocytic
265 lymphohistiocytosis in humanized mice', *Blood*, 117(21), pp. 5663–5673. Available at:
266 https://doi.org/10.1182/blood-2010-09-305979.

267 Schmidt, J. *et al.* (2003) 'Treatment and prevention of experimental autoimmune neuritis with
268 superagonistic CD28-specific monoclonal antibodies', *Journal of Neuroimmunology*, 140(1), pp. 143–
269 152. Available at: https://doi.org/10.1016/S0165-5728(03)00182-6.

270 Schneider-Hohendorf, T. *et al.* (2022) 'Broader Epstein–Barr virus–specific T cell receptor repertoire in
271 patients with multiple sclerosis', *The Journal of Experimental Medicine*, 219(11), p. e20220650. Available
272 at: https://doi.org/10.1084/jem.20220650.

273 Serafini, B. *et al.* (2004) 'Detection of Ectopic B-cell Follicles with Germinal Centers in the Meninges of
274 Patients with Secondary Progressive Multiple Sclerosis', *Brain Pathology*, 14(2), pp. 164–174. Available
275 at: https://doi.org/10.1111/j.1750-3639.2004.tb00049.x.

276 Serafini, B. *et al.* (2007) 'Dysregulated Epstein-Barr virus infection in the multiple sclerosis brain', *The*
277 *Journal of Experimental Medicine*, 204(12), pp. 2899–2912. Available at:
278 https://doi.org/10.1084/jem.20071030.

279 Simmons, S.B. *et al.* (2013) 'Modeling the Heterogeneity of Multiple Sclerosis in Animals', *Trends in*
280 *immunology*, 34(8), pp. 410–422. Available at: https://doi.org/10.1016/j.it.2013.04.006.

281 Staras, S.A.S. *et al.* (2006) 'Seroprevalence of Cytomegalovirus Infection in the United States, 1988–
282 1994', *Clinical Infectious Diseases*, 43(9), pp. 1143–1151. Available at: https://doi.org/10.1086/508173.

283 Suntharalingam, G. *et al.* (2006) 'Cytokine storm in a phase 1 trial of the anti-CD28 monoclonal antibody
284 TGN1412', *The New England Journal of Medicine*, 355(10), pp. 1018–1028. Available at:
285 https://doi.org/10.1056/NEJMoa063842.

286 Thacker, E.L., Mirzaei, F. and Ascherio, A. (2006) 'Infectious mononucleosis and risk for multiple
287 sclerosis: A meta-analysis', *Annals of Neurology*, 59(3), pp. 499–503. Available at:
288 https://doi.org/10.1002/ana.20820.

289 Unterweger, A.-L. *et al.* (2021) 'NOD/scid IL-2Rγnull mice reconstituted with peripheral blood
290 mononuclear cells from patients with Crohn's disease reflect the human pathological phenotype',
291 *Immunity, Inflammation and Disease*, 9(4), pp. 1631–1647. Available at: https://doi.org/10.1002/iid3.516.

292 Wagner, C.A. *et al.* (2020) 'Myelin-specific CD8+ T cells exacerbate brain inflammation in CNS
293 autoimmunity', *The Journal of Clinical Investigation*, 130(1), pp. 203–213. Available at:
294 https://doi.org/10.1172/JCI132531.

295 Wang, J. *et al.* (2020) 'HLA-DR15 Molecules Jointly Shape an Autoreactive T Cell Repertoire in Multiple
296 Sclerosis', *Cell*, 0(0). Available at: https://doi.org/10.1016/j.cell.2020.09.054.

297 Warner, H.B. and Carp, R.I. (1981) 'MULTIPLE SCLEROSIS AND EPSTEIN-BARR VIRUS', *The*
298 *Lancet*, 318(8258), p. 1290. Available at: https://doi.org/10.1016/S0140-6736(81)91527-0.

299 Yajima, M. *et al.* (2008) 'A New Humanized Mouse Model of Epstein-Barr Virus Infection That
300 Reproduces Persistent Infection, Lymphoproliferative Disorder, and Cell-Mediated and Humoral Immune
301 Responses', *Journal of Infectious Diseases*, 198(5), pp. 673–682. Available at:
302 https://doi.org/10.1086/590502.

303 Yamasaki, R. *et al.* (2014) 'Differential roles of microglia and monocytes in the inflamed central nervous
304 system', *Journal of Experimental Medicine*, 211(8), pp. 1533–1549. Available at:
305 https://doi.org/10.1084/jem.20132477.

306 Zayoud, M. *et al.* (2013) 'Subclinical CNS Inflammation as Response to a Myelin Antigen in Humanized
307 Mice', *Journal of Neuroimmune Pharmacology*, 8(4), pp. 1037–1047. Available at:
308 https://doi.org/10.1007/s11481-013-9466-4.

309 Zdimerova, H. *et al.* (2020) 'Attenuated immune control of Epstein Barr virus in humanized mice is
310 associated with the multiple sclerosis risk factor HLA-DR15', *European Journal of Immunology*
311 [Preprint]. Available at: https://doi.org/10.1002/eji.202048655.

312 Zhang, J. *et al.* (2021) 'Human Microglia Extensively Reconstitute in Humanized-BLT Mice With Human
313 Interleukin-34 Transgene and Support HIV-1 Brain Infection', *Frontiers in Immunology*, 12, p. 672415.
314 Available at: https://doi.org/10.3389/fimmu.2021.672415.

315

Figure 1

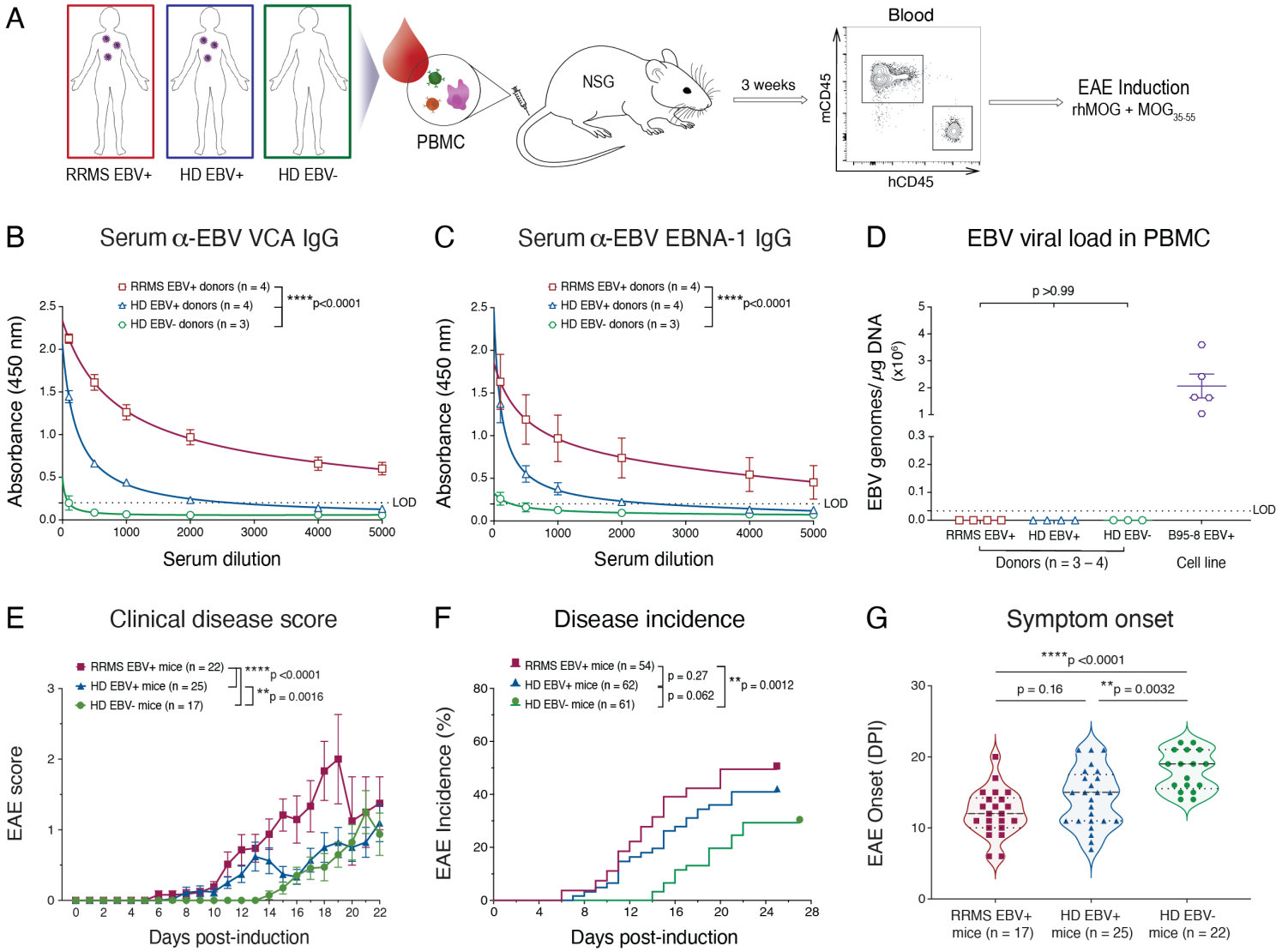
A
RRMS EBV+
HD EBV+
HD EBV-
PBMC
NSG
3 weeks
Blood
mCD45
hCD45
EAE Induction
rhMOG + MOG35-55
B
Serum α-EBV VCA IgG
RRMS EBV+ donors (n = 4)
HD EBV+ donors (n = 4)
HD EBV- donors (n = 3)
****p<0.0001
Absorbance (450 nm)
LOD
Serum dilution
C
Serum α-EBV EBNA-1 IgG
RRMS EBV+ donors (n = 4)
HD EBV+ donors (n = 4)
HD EBV- donors (n = 3)
****p<0.0001
Absorbance (450 nm)
LOD
Serum dilution
D
EBV viral load in PBMC
p >0.99
EBV genomes/ μg DNA (x10^6)
LOD
RRMS EBV+
HD EBV+
HD EBV-
B95-8 EBV+
Donors (n = 3 – 4)
Cell line
E
Clinical disease score
RRMS EBV+ mice (n = 22)
HD EBV+ mice (n = 25)
HD EBV- mice (n = 17)
****p <0.0001
**p = 0.0016
EAE score
Days post-induction
F
Disease incidence
RRMS EBV+ mice (n = 54)
HD EBV+ mice (n = 62)
HD EBV- mice (n = 61)
p = 0.27
p = 0.062
**p = 0.0012
EAE Incidence (%)
Days post-induction
G
Symptom onset
****p <0.0001
p = 0.16
**p = 0.0032
EAE Onset (DPI)
RRMS EBV+ mice (n = 17)
HD EBV+ mice (n = 25)
HD EBV- mice (n = 22)

Table 1

Donor ID	Age (years)	Age (years) at MS symptom onset	EDSS score	Disease duration	EBV IgG serostatus	CMV IgG serostatus	Serum 25-OH (ng/mL)
MS-01	24	24	2.5	4 months	VCA + EBNA-1 +	+	29.7
MS-02	31	31	2.5	6 months	VCA + EBNA-1 -	+	34.9
MS-03	32	26	2.0	5 years	VCA + EBNA-1 +	-	19.9
MS-04	39	31	2.0	7 years	VCA + EBNA-1 +	-	66.5
HD-01	39	N/A	N/A	N/A	VCA + EBNA-1 +	-	27.7
HD-02	25	N/A	N/A	N/A	VCA - EBNA-1 -	-	35.0
HD-03	26	N/A	N/A	N/A	VCA - EBNA-1 -	-	29.8
HD-04	23	N/A	N/A	N/A	VCA + EBNA-1 +	+	37.5
HD-05	19	N/A	N/A	N/A	VCA - EBNA-1 -	+	18.9
HD-06	25	N/A	N/A	N/A	VCA + EBNA-1 -	+	38.4
HD-07	28	N/A	N/A	N/A	VCA + EBNA-1 +	-	27.5

Figure 2

Spinal cord

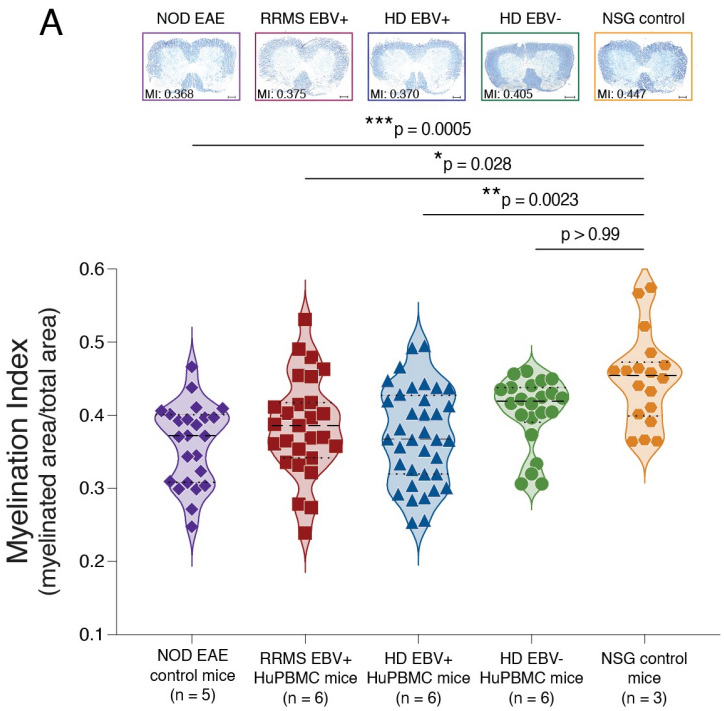

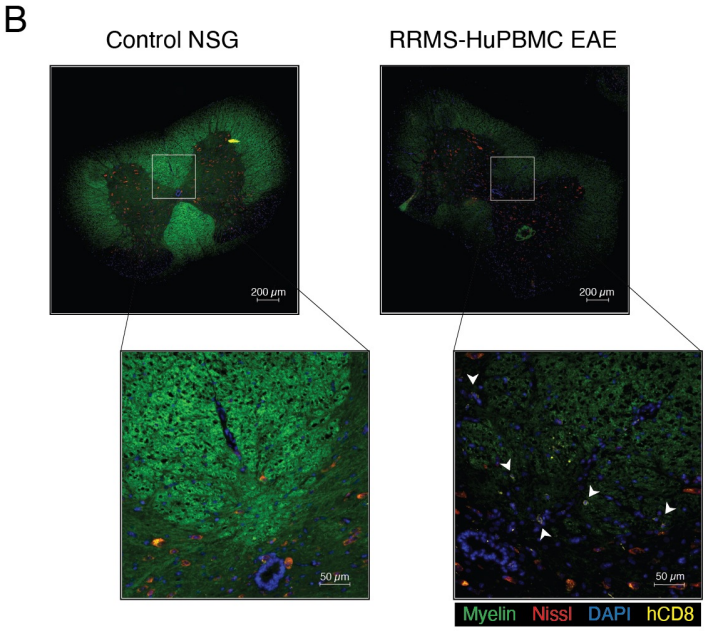

Cerebellum

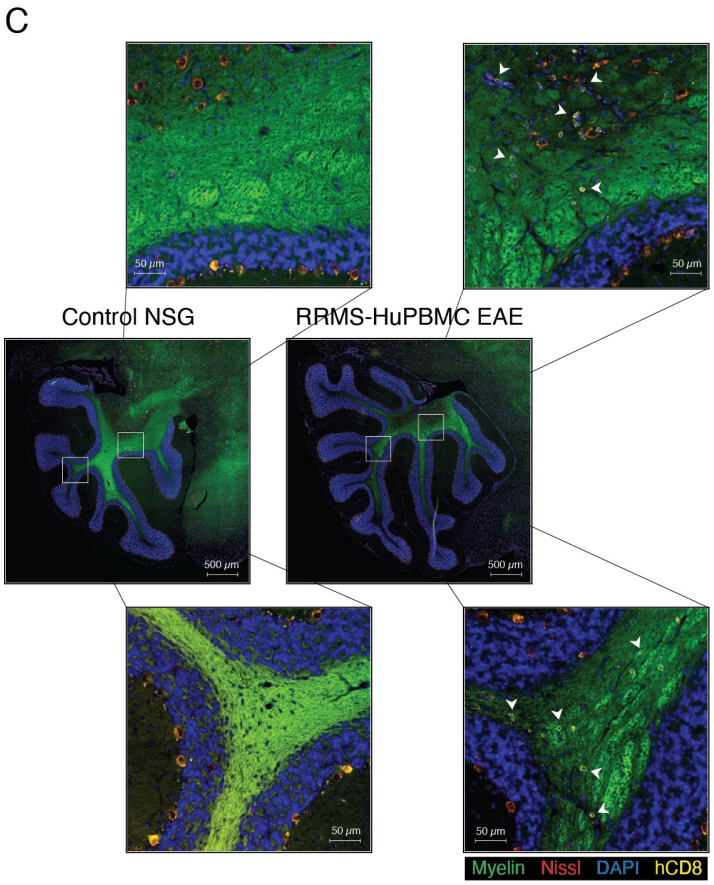

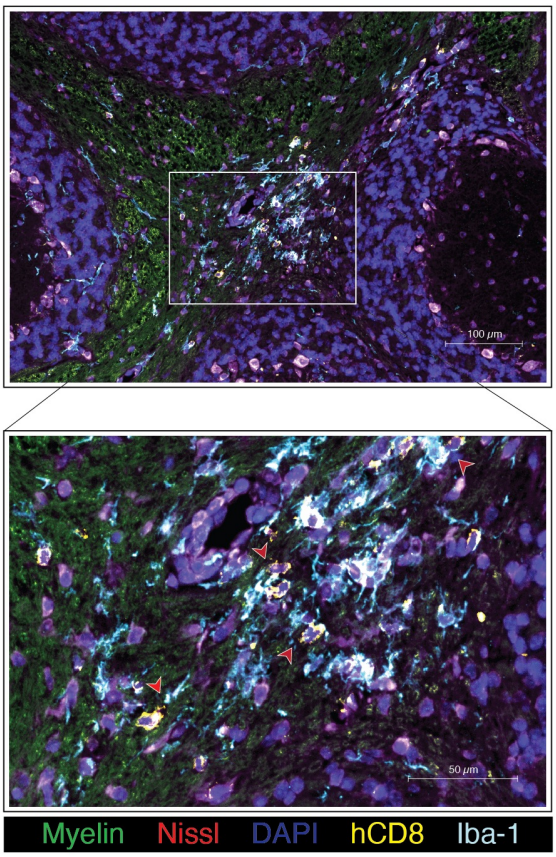

Figure 3

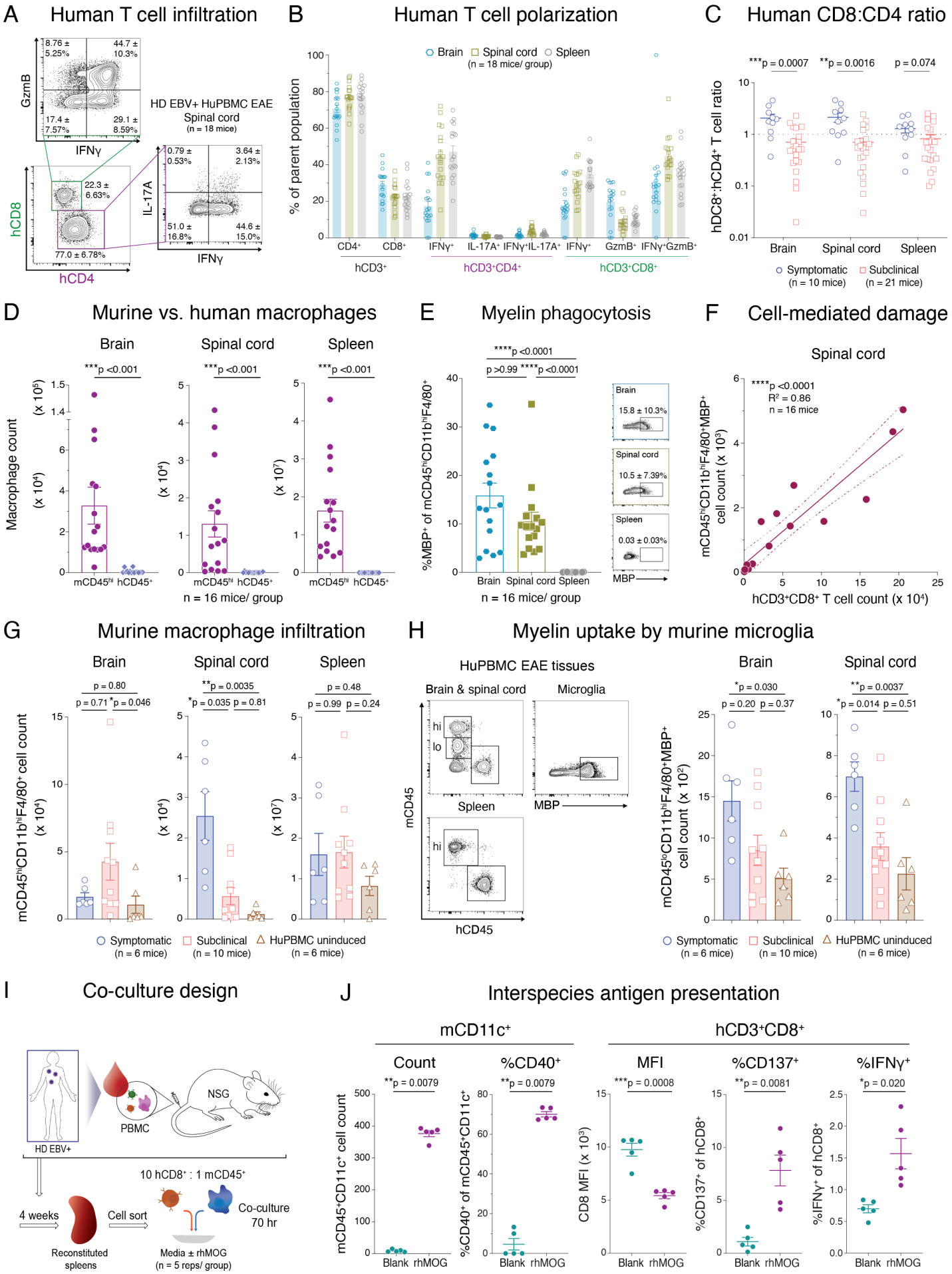
A Human T cell infiltration
HD EBV+ HuPBMC EAE
Spinal cord
(n = 18 mice)
GzmB
IFNγ
hCD8
hCD4
IL-17A
8.76 ± 5.25%
44.7 ± 10.3%
17.4 ± 7.57%
29.1 ± 8.59%
22.3 ± 6.63%
77.0 ± 6.78%
0.79 ± 0.53%
3.64 ± 2.13%
51.0 ± 16.8%
44.6 ± 15.0%
B Human T cell polarization
Brain
Spinal cord
Spleen
(n = 18 mice/ group)
% of parent population
CD4+
CD8+
IFNγ+
IL-17A+
IFNγ+IL-17A+
GzmB+
IFNγ+GzmB+
hCD3+
hCD3+CD4+
hCD3+CD8+
C Human CD8:CD4 ratio
***p = 0.0007
**p = 0.0016
p = 0.074
hDC8+:hCD4+ T cell ratio
Brain
Spinal cord
Spleen
Symptomatic (n = 10 mice)
Subclinical (n = 21 mice)
D Murine vs. human macrophages
Brain
Spinal cord
Spleen
***p <0.001
Macrophage count
mCD45hi
hCD45+
n = 16 mice/ group
E Myelin phagocytosis
****p <0.0001
p >0.99
%MBP+ of mCD45hiCD11bhiF4/80+
Brain
Spinal cord
Spleen
15.8 ± 10.3%
10.5 ± 7.39%
0.03 ± 0.03%
MBP
n = 16 mice/ group
F Cell-mediated damage
Spinal cord
****p <0.0001
R2 = 0.86
n = 16 mice
mCD45hiCD11bhiF4/80+MBP+ cell count (x 103)
hCD3+CD8+ T cell count (x 104)
G Murine macrophage infiltration
Brain
Spinal cord
Spleen
p = 0.80
p = 0.71
*p = 0.046
**p = 0.0035
*p = 0.035
p = 0.81
p = 0.48
p = 0.99
p = 0.24
mCD45hiCD11bhiF4/80+ cell count
Symptomatic (n = 6 mice)
Subclinical (n = 10 mice)
HuPBMC uninduced (n = 6 mice)
H Myelin uptake by murine microglia
HuPBMC EAE tissues
Brain & spinal cord
Microglia
hi
lo
Spleen
MBP
mCD45
hCD45
Brain
Spinal cord
*p = 0.030
p = 0.20
p = 0.37
**p = 0.0037
*p = 0.014
p = 0.51
mCD45loCD11bhiF4/80+MBP+ cell count (x 102)
Symptomatic (n = 6 mice)
Subclinical (n = 10 mice)
HuPBMC uninduced (n = 6 mice)
I Co-culture design
HD EBV+
PBMC
NSG
10 hCD8+ : 1 mCD45+
4 weeks
Cell sort
Co-culture 70 hr
Reconstituted spleens
Media ± rhMOG (n = 5 reps/ group)
J Interspecies antigen presentation
mCD11c+
hCD3+CD8+
Count
%CD40+
MFI
%CD137+
%IFNγ+
**p = 0.0079
**p = 0.0079
***p = 0.0008
**p = 0.0081
*p = 0.020
mCD45+CD11c+ cell count
%CD40+ of mCD45+CD11c+
CD8 MFI (x 103)
%CD137+ of hCD8+
%IFNγ+ of hCD8+
Blank
rhMOG

Figure 4

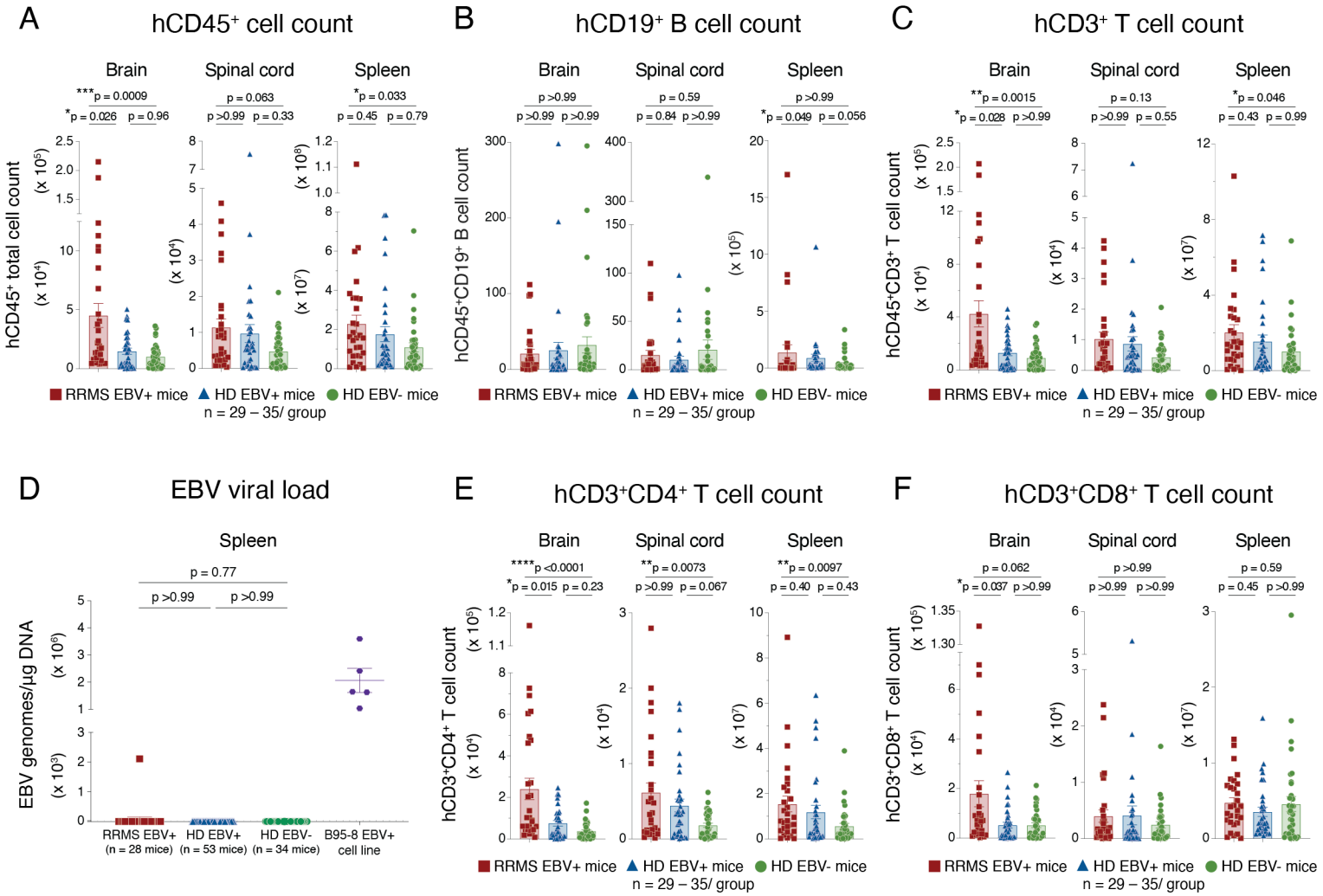
A
hCD45+ cell count
Brain
Spinal cord
Spleen
***p = 0.0009
*p = 0.026
p = 0.96
p = 0.063
p >0.99
p = 0.33
*p = 0.033
p = 0.45
p = 0.79
hCD45+ total cell count
(x 10^5)
(x 10^4)
(x 10^4)
(x 10^8)
(x 10^7)
RRMS EBV+ mice
HD EBV+ mice
HD EBV- mice
n = 29 – 35/ group
B
hCD19+ B cell count
Brain
Spinal cord
Spleen
p >0.99
p >0.99
p >0.99
p = 0.59
p = 0.84
p >0.99
p >0.99
*p = 0.049
p = 0.056
hCD45+CD19+ B cell count
(x 10^5)
RRMS EBV+ mice
HD EBV+ mice
HD EBV- mice
n = 29 – 35/ group
C
hCD3+ T cell count
Brain
Spinal cord
Spleen
**p = 0.0015
*p = 0.028
p >0.99
p = 0.13
p >0.99
p = 0.55
*p = 0.046
p = 0.43
p = 0.99
hCD45+CD3+ T cell count
(x 10^5)
(x 10^4)
(x 10^4)
(x 10^7)
RRMS EBV+ mice
HD EBV+ mice
HD EBV- mice
n = 29 – 35/ group
D
EBV viral load
Spleen
p = 0.77
p >0.99
p >0.99
EBV genomes/µg DNA
(x 10^6)
(x 10^3)
RRMS EBV+ (n = 28 mice)
HD EBV+ (n = 53 mice)
HD EBV- (n = 34 mice)
B95-8 EBV+ cell line
E
hCD3+CD4+ T cell count
Brain
Spinal cord
Spleen
****p <0.0001
*p = 0.015
p = 0.23
**p = 0.0073
p >0.99
p = 0.067
**p = 0.0097
p = 0.40
p = 0.43
hCD3+CD4+ T cell count
(x 10^5)
(x 10^4)
(x 10^4)
(x 10^7)
RRMS EBV+ mice
HD EBV+ mice
HD EBV- mice
n = 29 – 35/ group
F
hCD3+CD8+ T cell count
Brain
Spinal cord
Spleen
p = 0.062
*p = 0.037
p >0.99
p >0.99
p >0.99
p = 0.59
p = 0.45
p >0.99
hCD3+CD8+ T cell count
(x 10^5)
(x 10^4)
(x 10^4)
(x 10^7)
RRMS EBV+ mice
HD EBV+ mice
HD EBV- mice
n = 29 – 35/ group

Figure 5

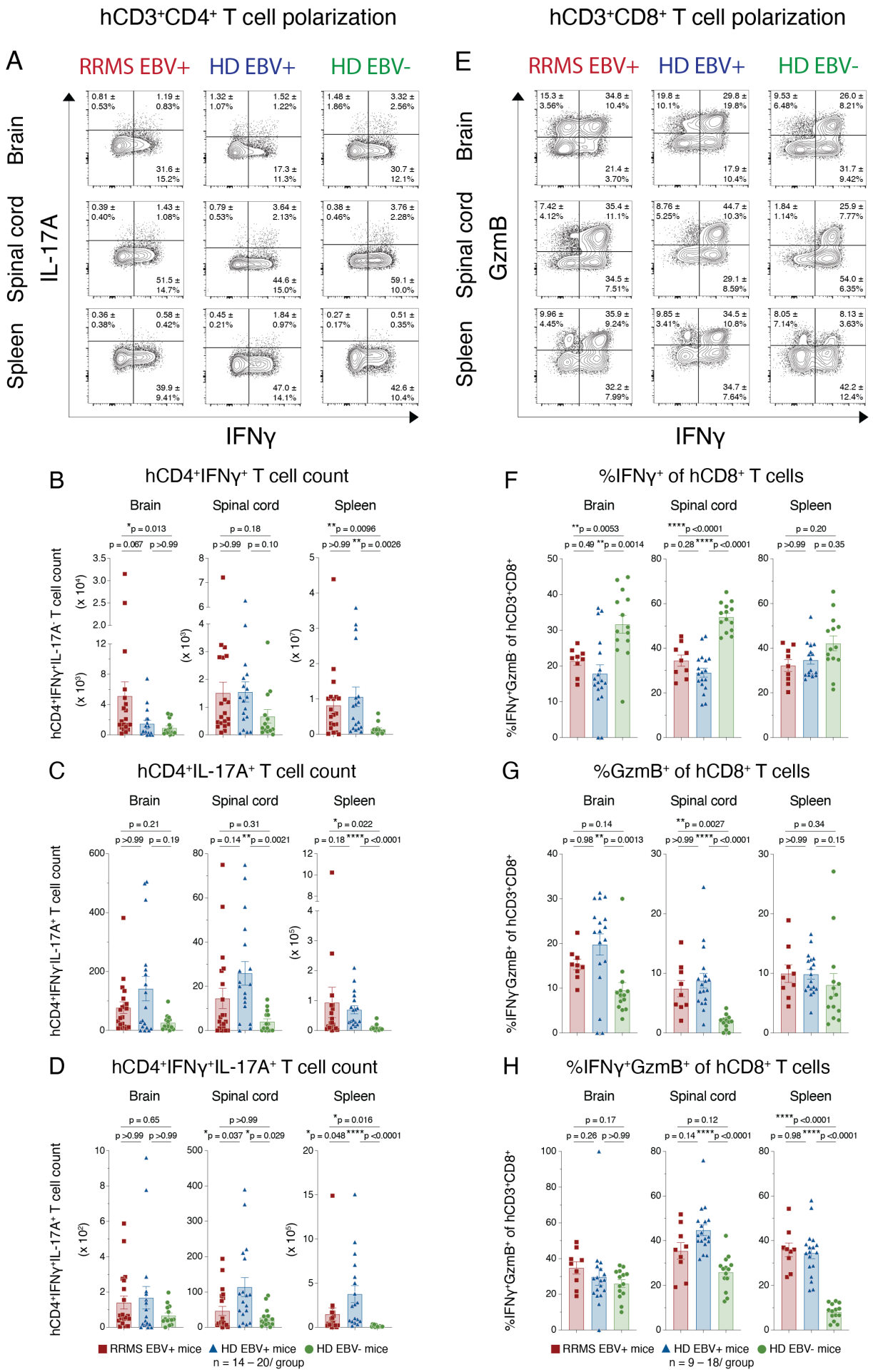
hCD3+CD4+ T cell polarization
hCD3+CD8+ T cell polarization
A
E
RRMS EBV+
HD EBV+
HD EBV-
Brain
Spinal cord
Spleen
IL-17A
GzmB
IFNγ
B
hCD4+IFNγ+ T cell count
F
%IFNγ+ of hCD8+ T cells
C
hCD4+IL-17A+ T cell count
G
%GzmB+ of hCD8+ T cells
D
hCD4+IFNγ+IL-17A+ T cell count
H
%IFNγ+GzmB+ of hCD8+ T cells
hCD4+IFNγ+IL-17A- T cell count
%IFNγ+GzmB- of hCD3+CD8+
%IFNγ-GzmB+ of hCD3+CD8+
RRMS EBV+ mice
HD EBV+ mice
HD EBV- mice
n = 14 – 20/ group
n = 9 – 18/ group

Figure 6

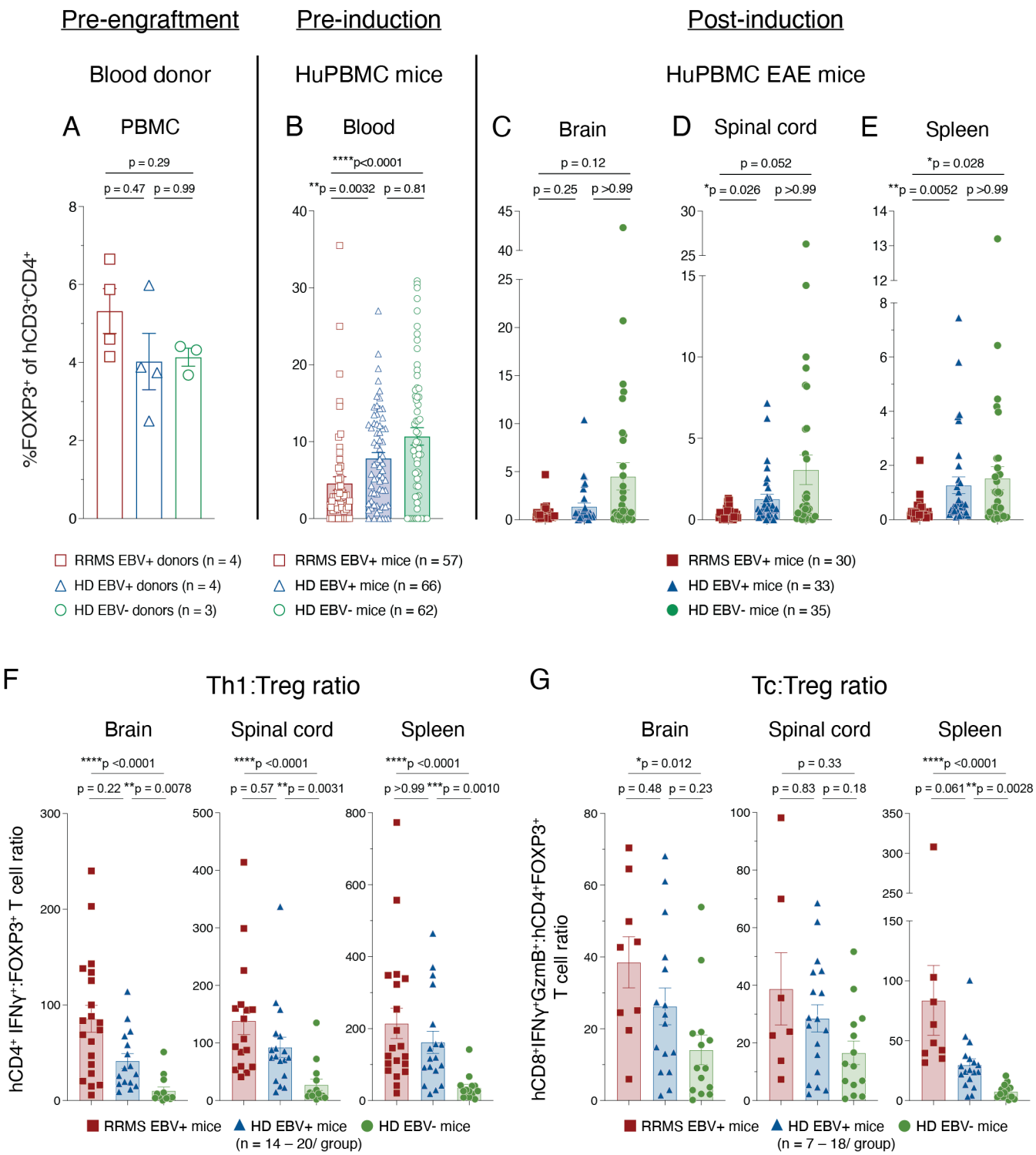
Pre-engraftment
Pre-induction
Post-induction
Blood donor
HuPBMC mice
HuPBMC EAE mice
A PBMC
B Blood
C Brain
D Spinal cord
E Spleen
%FOXP3+ of hCD3+CD4+
p = 0.29
p = 0.47 p = 0.99
****p<0.0001
**p = 0.0032 p = 0.81
p = 0.12
p = 0.25 p >0.99
p = 0.052
*p = 0.026 p >0.99
*p = 0.028
**p = 0.0052 p >0.99
RRMS EBV+ donors (n = 4)
HD EBV+ donors (n = 4)
HD EBV- donors (n = 3)
RRMS EBV+ mice (n = 57)
HD EBV+ mice (n = 66)
HD EBV- mice (n = 62)
RRMS EBV+ mice (n = 30)
HD EBV+ mice (n = 33)
HD EBV- mice (n = 35)
F Th1:Treg ratio
Brain
Spinal cord
Spleen
hCD4+ IFNγ+:FOXP3+ T cell ratio
****p <0.0001
p = 0.22 **p = 0.0078
****p <0.0001
p = 0.57 **p = 0.0031
****p <0.0001
p >0.99 ***p = 0.0010
RRMS EBV+ mice
HD EBV+ mice
HD EBV- mice
(n = 14 – 20/ group)
G Tc:Treg ratio
Brain
Spinal cord
Spleen
hCD8+IFNγ+GzmB+:hCD4+FOXP3+ T cell ratio
*p = 0.012
p = 0.48 p = 0.23
p = 0.33
p = 0.83 p = 0.18
****p <0.0001
p = 0.061 **p = 0.0028
RRMS EBV+ mice
HD EBV+ mice
HD EBV- mice
(n = 7 – 18/ group)

Figure 7

α-hCD3/CD28 bead stimulated donor PBMC

hCD3⁺CD4⁺ T cells

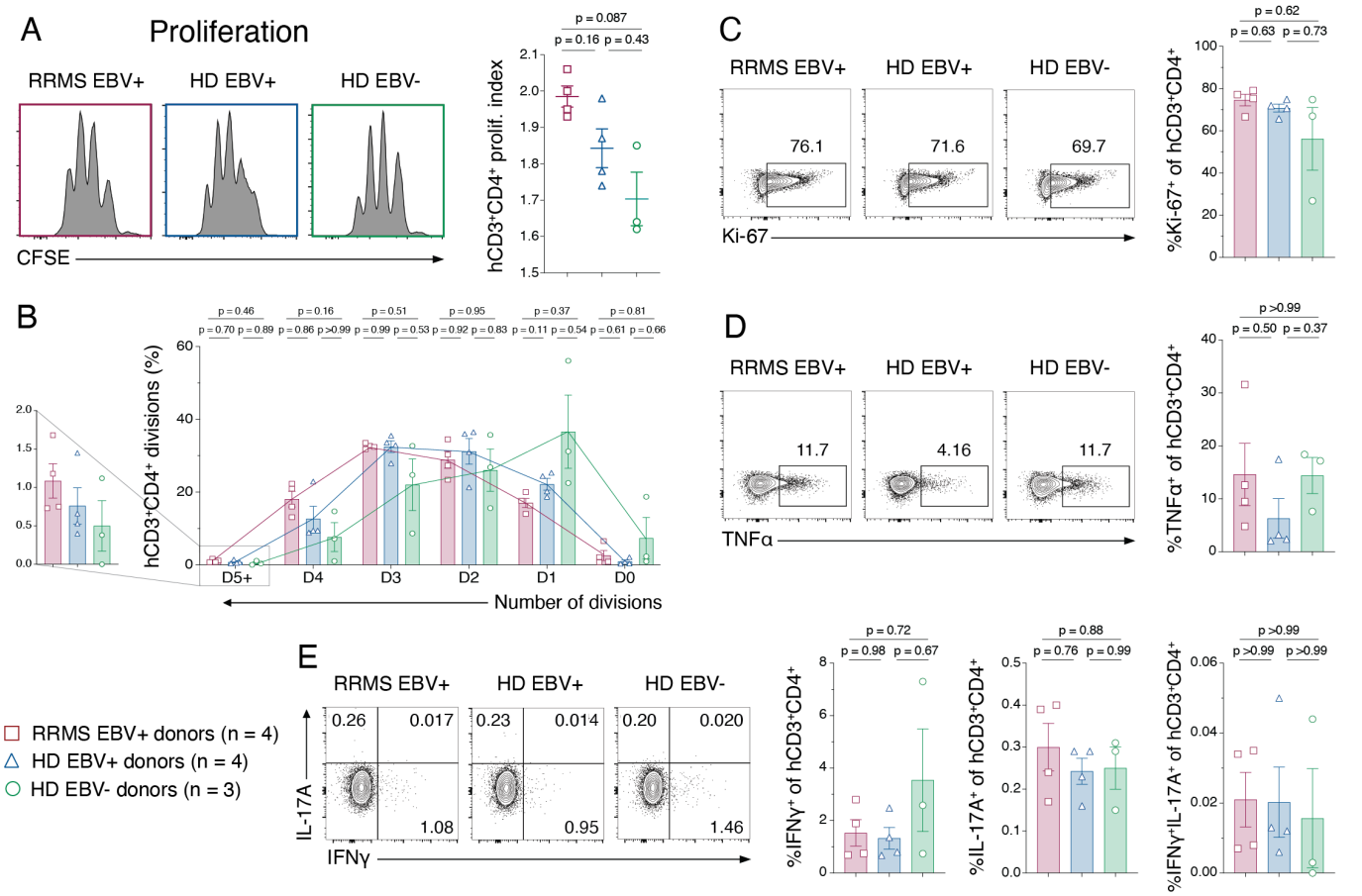
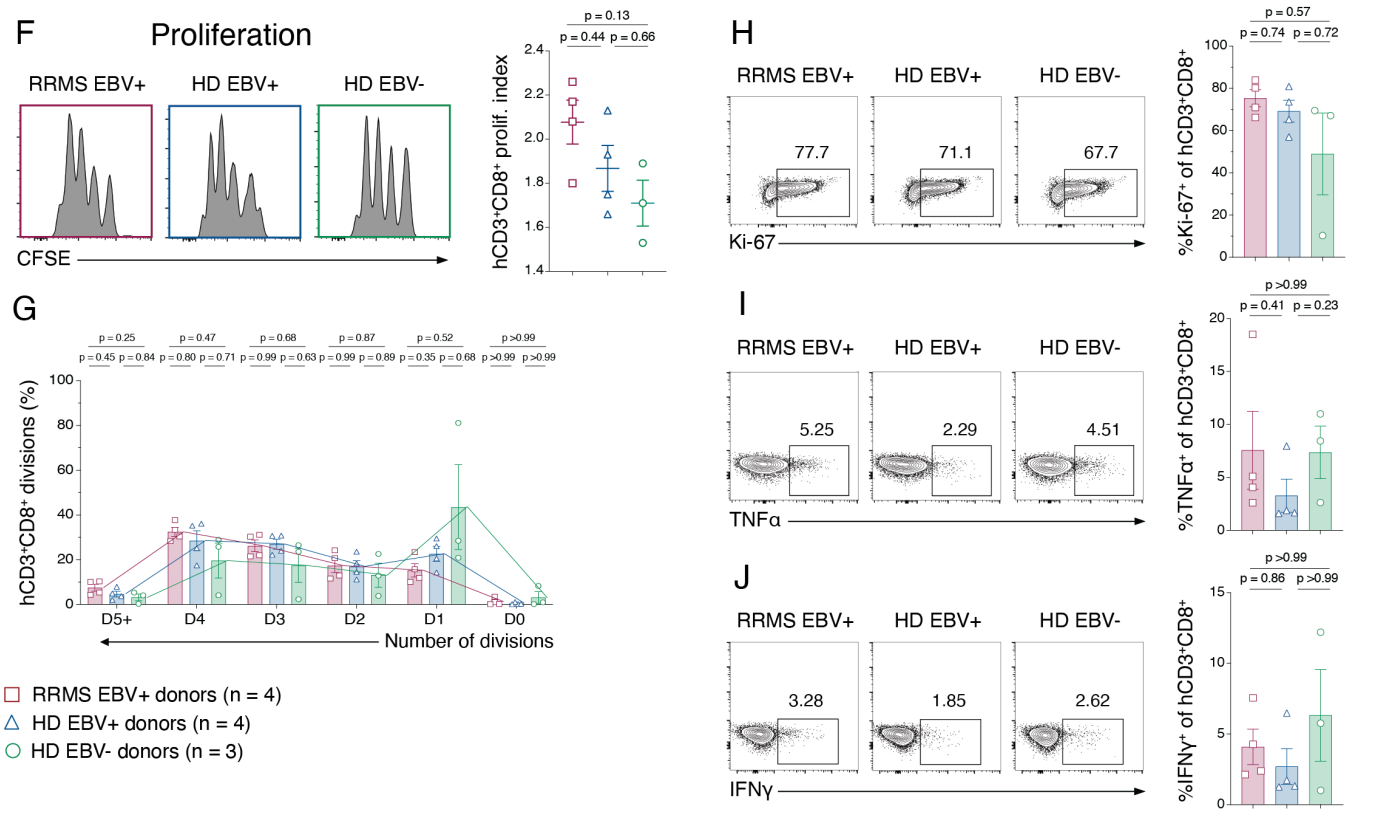
hCD3⁺CD8⁺ T cells